Compass-Like Biped Robot Part I : Stability and Bifurcation of Passive Gaits

Ambarish Goswami, Benoît Thuilot, Bernard Espiau

INRIA

INSTITUT NATIONAL DE RECHERCHE EN INFORMATIQUE ET EN AUTOMATIQUE

Compass-like biped robot
Part I: Stability and bifurcation of passive gaits

Ambarish Goswami, Benoit Thuilot, Bernard Espiau

N ° 2996

October 1996

THÈME 4

ISSN 0249-6399

INRIA
RHÔNE-ALPES

Compass-like biped robot
Part I: Stability and bifurcation of passive gaits

Ambarish Goswami, Benoit Thuilot, Bernard Espiau

Thème 4 — Simulation et optimisation
de systèmes complexes
Projet BIP

Rapport de recherche n ° 2996 — October 1996 — 86 pages

Abstract: It is well-known that a suitably designed unpowered mechanical biped robot can "walk" down an inclined plane with a steady gait. The characteristics of the gait (e.g., velocity, step period, step length) depend on the geometry and the inertial properties of the robot and the slope of the plane. The energy required to maintain the steady motion comes from the conversion of the biped's gravitational potential energy as it descends. Investigation of such passive "natural" motions may potentially lead us to strategies useful for controlling active walking machines as well as to understand human locomotion.

In this report we demonstrate the existence and the stability of symmetric and asymmetric passive gaits using a simple nonlinear biped robot model. Kinematically the robot is identical to a double pendulum (similar to the Acrobot and the Pendubot) and is able to walk with the so-called *compass gait*. We also identify period-doubling bifurcation in this passive gait which eventually leads to a chaotic regime for larger slopes.

Key-words: Biped robot, Compass gait, Passive gait, Phase plane diagram, Orbital stability, Poincaré mapping, Bifurcation, Chaotic behavior

(Résumé : tsvp)

Unité de recherche INRIA Rhône-Alpes
655, avenue de l'Europe, 38330 MONTBONNOT ST MARTIN (France)
Téléphone : (33) 76 61 52 00 – Télécopie : (33) 76 61 52 52

Etude d'un robot bipède de type compas
Partie I: analyse de la stabilité et des bifurcations des régimes de marche passive

Résumé : Il a été prouvé qu'il est possible de construire des robots bipèdes pouvant "marcher" pendant un temps infini le long de plans inclinés descendants, sans être actionnés. Les caractéristiques de cette marche (c'est-à-dire la vitesse, la période, la longueur du pas,...) sont fonction des propriétés géométriques et inertielles du robot et de l'inclinaison du sol. L'énergie permettant au robot de marcher ainsi indéfiniment provient simplement de la conversion, au fur et à mesure de la descente, de l'énergie potentielle de pesanteur du robot en énergie cinétique. L'étude de telles marches "naturelles" et complètement passives présente un intérêt, d'une part pour concevoir des stratégies de commande pour des robots marcheurs qui seraient cette fois actionnés, et d'autre part pour mieux comprendre la marche humaine.

Dans ce rapport, nous nous sommes intéressés à un modèle non-linéaire simple de robot bipède. D'un point de vue cinématique, le système considéré est identique à un double-pendule (comme les robots Acrobot et Pendubot) et peut marcher avec *l'allure dite du Compas.* Nous avons étudié l'existence et la stabilité de régimes de marche passive symétriques et asymétriques. Pour certaines valeurs de l'inclinaison du sol et/ou pour certaines répartitions de masses sur le robot, nous avons également identifié des bifurcations de type "doublement de période" aboutissant à des régimes chaotiques.

Mots-clé : Robot bipède, Allure de marche "Compas", Marche passive, Diagramme de phase, Stabilité orbitale, Section de Poincaré, Bifurcation, Régime chaotique

Contents

List of Figures

Nomenclature

Symbol	Definition	First use
	Convention	
	matrices are written using capital boldfaced characters vectors are written using small boldfaced characters scalars are written using lightfaced characters	
	Roman	
$\boldsymbol{A}$	4×4 state matrix of the linearized biped model	p. 29
a	distance between leg tip and lumped mass m	p. 13
b	distance between hip and lumped mass m	p. 13
$\boldsymbol{D}(\alpha, T)$	4×4 step-to-step matrix	p. 31
E	mechanical energy of the biped robot	p. 17
ΔE	mechanical energy lost during leg impact	p. 18
g	acceleration due to gravity: $g = 9.81$ m.s^{-2}	p. 50
$\boldsymbol{g}(\boldsymbol{\theta})$	2×1 gravity torque vector	p. 16
$\boldsymbol{g}_n(\boldsymbol{\theta})$	2×1 gravity torque vector for the normalized equations	p. 18
$\boldsymbol{G}_0$	2×2 gravity torque matrix when $\boldsymbol{\theta} \approx 0$ ($\boldsymbol{g}(\boldsymbol{\theta}) \approx \boldsymbol{G}_0\boldsymbol{\theta}$)	p. 52
$\boldsymbol{H}(\alpha)$	2×2 transition submatrix, associated to angular velocities	p. 17
$\boldsymbol{I}_n$	$n \times n$ identity matrix	p. 25
$\boldsymbol{J}$	2×2 skew-symmetric matrix	p. 17
K	kinetic energy of the biped robot	p. 23
l	leg length ($l = a + b$)	p. 13
L	step length	p. 15
$\boldsymbol{M}(\boldsymbol{\theta})$	2×2 inertia matrix	p. 16
$\boldsymbol{M}_n(\boldsymbol{\theta})$	2×2 inertia matrix for the normalized equations	p. 18
$\boldsymbol{M}_0$	inertia matrix for $\boldsymbol{\theta} = 0$ ($\boldsymbol{M}_0 = \boldsymbol{M}_{(\boldsymbol{\theta}=\boldsymbol{0})}$)	p. 52
m	lumped mass of each leg	p. 13
m_H	lumped mass of the hip	p. 13
m_C	total mass of the robot	p. 13
$\boldsymbol{N}(\boldsymbol{\theta}, \dot{\boldsymbol{\theta}})$	2×2 centrifugal and Coriolis matrix	p. 16

Symbol	Definition	First use
$\boldsymbol{N}_n(\boldsymbol{\theta},\dot{\boldsymbol{\theta}})$	2×2 centrifugal and Coriolis matrix for the normalized equations	p. 18
P	potential energy of the biped robot	p. 23
$\boldsymbol{q}$	$[\theta_{ns} \;\; \theta_s \;\; \dot{\theta}_{ns} \;\; \dot{\theta}_s]^T$: state vector of the biped model	p. 15
$\boldsymbol{Q}$	2×2 matrix providing angular momenta	p. 53
$\boldsymbol{Q}_n$	2×2 matrix providing angular momenta for the normalized equations	p. 53
T	step period	p. 15
v	average speed of progression (ASP) of the biped	p. 15
$\boldsymbol{W}(\alpha)$	4×4 transition matrix	p. 17
	Greek	
α	half-inter-leg angle	p. 15
β	length ratio: b divided by a	p. 13
η	angular velocities ratio: $\dot{\theta}_{ns}$ divided by $\dot{\theta}_s$	p. 58
θ	leg angle with respect to the vertical	p. 15
$\boldsymbol{\theta}$	$[\theta_{ns} \;\; \theta_s]^T$: generalized coordinates of the biped	p. 15
μ	mass ratio: m_H divided by m	p. 13
ϕ	ground slope	p. 13
	Superscript	
$^-$	value of a variable just before a leg impact	p. 17
$^+$	value of a variable just after a leg impact	p. 17
*	value of a variable during a steady gait	p. 25
$'$	biped reference mass or length (for simulations)	p. 18
	Subscript	
$_H$	variable related to the hip	p. 13
$_k$	step counter	p. 15
$_{ns}$	variable related to the non-support (or swing) leg	p. 15
$_s$	variable related to the support leg	p. 15

1 Why study passive compass gait?

Biped locomotion is one of the most sophisticated forms of legged motion. From a dynamic systems point of view, human locomotion stands out among other forms of biped locomotion chiefly due to the fact that during a significant part of the human walking cycle the moving body is not in the static equilibrium. At the INRIA Rhône-Alpes laboratory of Grenoble, France, we are working on the development of an anthropomorphic biped walker. The envisioned prototype will have reasonable adaptation capability on an unforeseen uneven terrain. The purpose of the project is not limited to the realization of a complex machine, the construction and control of which nevertheless pose formidable engineering challenge. We also intend to initiate a synergy between robotics and human gait study. Human locomotion, despite being well studied and enjoying a rich database, is not well understood and a robotic simulcrum potentially can be very useful.

In order to gain a better understanding of the inherently nonlinear dynamics of a full-fledged walking machine we have found it instructive to first explore the behavior of a particularly simple, perhaps the simplest, walker model. Inspired by the research of [GH77] and [BWH83], and the relatively more recent research on passive walking machines [McG90] we have considered the model of a so-called "compass gait" walker. Based on the same kinematics as that of a double pendulum, the Acrobot [BF92], [Spo95] and the Pendubot [BS95] are the nearest cousins of our compass gait model. McGeer[McG90] designed several unpowered biped robots and studied their gravity-induced passive motion on inclined planes. He demonstrated that the prototype can attain a stable steady periodic motion and analyzed this behavior with a linearized mathematical model. In order to maintain a steady periodic locomotion the joint variables (angle, velocity) of the robot must follow a steady cyclic trajectory. Our objective is to study such a passive system by means of its full nonlinear equations and using tools available for nonlinear systems analysis. We have recently come across the work of [GCCR96] who employ a perturbation method to study a simple biped model in some limiting cases as some of the robot parameters tend to zero.

Underlying this somewhat local objective of studying elementary biped robot models there are several long term motivations all connected to the eventual goal of obtaining a simple biologically-inspired adaptive control law for our future prototype. The first is our intuitive support for the conjecture that legged locomotion and possibly all inter-limb coordinations are identified by nonlinear limit cycle oscillatory processes [KHRK81]. Next, a passive motion has a special appeal because

it is *natural* and it does not require any external energy source. If an active control law closely mimics the behavior of a stable passive walk it is likely to enjoy certain inherent advantages of the passive system such as the energy optimality, periodicity, and stability. Of particular interest in this respect is the hypothesis that a great part of the swing stage in human locomotion is passive, a hypothesis that is supported by many studies, for instance [McM84], and is utilized in biped robot research [GFLZ94].

It is shown here that passive compass gait is characterized by stable limit cycles in the phase space of the robot. The observed gait may be of symmetric or asymmetric step lengths or is chaotic. The particular gait adopted by the robot depends on the ground slope as well as on its geometric and inertial parameters. Using the dynamic systems jargon we can say that the chaotic gait of our robot results from a simple periodic behavior through a *cascade of period doubling bifurcations*. It is a common knowledge now that mathematically simple systems can exhibit a rich dynamic behavior and our compass-gait robot is a good example of this fact.

Although the robot model is mechanically simple, its governing equations are *hybrid* in the sense that they are nonlinear ordinary differential equations combined with algebraic switching conditions. This makes it difficult for us to utilize the traditional tools (such as the automatic detection of limit cycles [PC89]) developed for the study of nonlinear systems. Moreover, since the state-space of the robot is 4-dimensional we cannot take advantage of the visual depiction of the system trajectories.

There are several approaches that we can adopt in this situation. One approach, as was taken by McGeer [McG90] amongst others, is to linearize the dynamic equation of the robot about an equilibrium point. This allows us to explicitly integrate the dynamic equations of the robot. Next the collision equations with the ground is added and the conditions for the existence of a periodic solution of this coupled system is found. In order to study the stability of this periodic solution a second linearization about the periodic solution is necessary. The problem with this approach is that the linear solution is valid only within a certain region around the point of linearization. We will show in this report that as we move away from this point the prediction of the long term system behavior becomes impossible.

A second approach, adopted in the recent work of [GCCR96], and in a few studies of monopod robots [VB90] [OB93] [Fra96], is to simplify the model of the robot so that some analytical insight into the simplified *nonlinear* model is available. A typical advantage is the reduction in the dimension of the system which is useful for graphical visualization. Also it is often possible to obtain an explicit expression

for the Poincaré map of the robot. Although frequently useful, the general validity of these simplified models of the biped robot is not clear.

In our current study we have thus decided to preserve the full non-linear equations of the robot. The disadvantage in this approach is that our exploration has to rely to a large extent on numerical simulations. This is compensated by the fact that the robot model is still rather simple and the computational burden is not serious. In addition, since our immediate objective is a systematic study of the passive behavior of the robot, the concerns for real-time control do not concern us.

In Section 2, we describe the geometry, the dynamic parameters, the simplifying assumptions, and the governing equations of the compass-like robot. Section 3 proposes a general overview of compass gait characteristics: Section 3.1 discusses, with the help of a phase plane diagram, a typical walk cycle of the passive robot on an inclined plane. The motion of the robot is continued indefinitely thanks to a delicate balance between the robot's kinetic and potential energies (Section 3.2). In Section 3.4, we establish that the compass-like robot can exhibit walk cycles which are locally orbitally stable. Results of systematic numerical simulations are presented in Section 4 to improve our understanding of the gait mechanism. We demonstrate, for example, that period doubling cascades progressively transform a periodic gait to a chaotic gait. The final Section 5 presents conclusions and the future work. Derivation of the governing equations of the robot and and the detailed exposition of some of the analyses are given in the appendices. The simulation plots appear in Appendix C.

2 The compass gait model

The analogy between human locomotion and the gait of a biped walking machine makes it convenient for us to use the terminology developed and employed in the study of human biomechanics. In this section we will first present the precise definitions of some of the terms which will be often used in the rest of this report. We then proceed to the modeling assumptions adopted here. Next we present the governing equations of the biped. Finally in Section 4 we discuss the normalization procedure of the governing equations which we use to our advantage during the numerical simulation.

2.1 Some definitions

Compass gait Compass gait model perhaps represents the most elementary model of biped locomotion. In this model the legs are rigid bars without knee and foot, connected by a frictionless hinge at the hip (more details given in the following section). The motion is assumed to be 2-dimensional. The Cartesian hip trajectory consists of a series of circular arcs centered around the point of contact of the support leg with the ground and having a radius equal to the length of the leg. The gait is so named since the locomotion produced with this model is analogous to the movement of a pair of compasses or dividers.

We can add a word here to justify our study of compass gait. Biomechanists explain the overall mechanism of human locomotion as the coordinated action of a set of simpler sub-actions, termed the *six determinants of gait* [McM84], [RG94]. The first and the most basic of them is the compass gait. When it is combined successively with the other five determinants, the energy efficiency of the gait improves and the gait becomes smoother.

To be exhaustive, we must add that compass gait cannot exist in reality, either biologically or in a machine. This is because the fact that the swing leg, since it does not have a knee, cannot actually clear the ground. This conceptual problem is avoided here by including a prismatic-jointed knee with a telescopically retractable massless lower leg. The swing leg is retracted during most of its motion, and it lengthens just when it is about to touch the ground. This solves the problem of foot clearance without affecting robot dynamics.

Passive locomotion If a walking machine does not utilize any form of actuation for its motion, the locomotion of the machine is said to be passive. From the dynamic systems point of view an unpowered machine is an *autonomous* system.

Steady gait This term is loosely used to mean that the robot can indefinitely continue to walk without falling down.

Gait step The gait step describes the period between the take-off of one foot from the ground and its subsequent landing. The *step period* and the *gait frequency* are respectively the time taken by a step and the number of steps taken per second.

Symmetric gait A gait is symmetric if any two consecutive steps are indistinguishable, i.e., all the spatio-temporal parameters exactly repeat themselves in each step. When a gait does not possess this property it is said to be *asymmetric*.

Periodic gait A gait is periodic if all the spatio-temporal parameters repeat themselves after every p steps. The integer p is called the *gait period*. For symmetric gaits $p = 1$.

Gait cycle In case of a p-periodic gait the gait cycle consists of p successive steps.

Chaotic gait A chaotic gait is characterized by its total aperiodicity. All of the features of chaotic regime as discussed in the nonlinear dynamic systems literature are directly applicable for a biped robot as we will see in Section 4.2.4.

2.2 Description of the system and modeling assumptions

For the following discussion please refer to the Fig. 2.1 where we present the sketch of a compass-like biped robot.

The modeling assumptions are listed below (the individual assumptions are marked for later reference):

- *Mass:* concentrated at 3 points (A1):
  - mass m_H at the hip,
  - masses m on each leg, located at distances a and b from respectively the leg tip and the hip.

  The total mass of the robot $m_C = 2m + m_h$ is constant and equal to 20 Kg, whereas the mass ratio $\mu = \frac{m_H}{m}$ will be varied from 0.1 to 10 during the simulation trials.

- *Leg:* the legs are identical (A2). The leg length $l = a + b$ is constant and equal to 1 meter, whereas the length ratio $\beta = \frac{b}{a}$. β will be varied from 0.1 to 10 during the simulation trials.

- *Actuation:* the robot is unactuated (A3).

- *Ground:* the robot walks down on a plane surface inclined at a constant angle ϕ with the horizontal.

- *Gait:* consists of the following two stages :
  - *Swing:* during this stage the robot hip pivots around the point of support on the ground of its *support leg*. The other leg, called the *non-support leg* or the *swing leg* swings forward (the compass robot in Fig. 2.1 is in swing stage). The tip of the support leg is assumed not to slip (A4). The robot behaves as a ballistic double-pendulum.
  - *Transition:* it occurs instantaneously when the swing leg touches the ground and previous support leg leaves the ground (A5).
- *Collision:* the impact of the swing leg with the ground is assumed to be inelastic and without sliding. This implies that during the instantaneous transition stage (see for instance [HC92]):
  - robot configuration remains unchanged (A6),
  - the angular momentum of the robot about the impacting foot as well as the angular momentum of the pre-impact support leg about the hip are

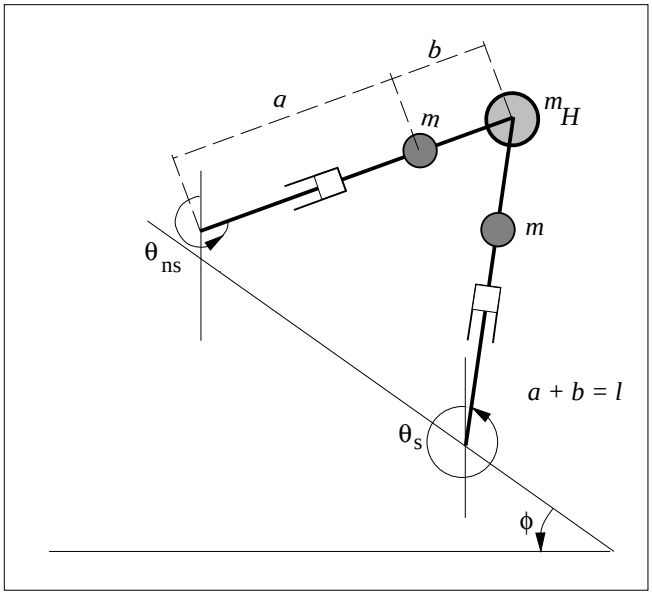

Figure 2.1: Model of a compass-like biped robot walking down a slope. Swing stage.

conserved (A7). These conservation laws lead to a discontinuous change in robot velocity.

- *Prismatic-joint knee:* a knee-less robot with a rigid leg cannot clear the ground. This conceptual problem is avoided here by including a prismatic-jointed knee with a massless lower leg, as mentioned before. Both legs have then same length l at the transition time.

  Our emphasis here is on the simplicity of the model than its physical realizability. Note however that robots of this type were developed and studied in [GFLZ94], [McG90].

We point out that the simplifying assumptions described here are routinely made in the biped robot literature (see [McG90],[HC92]) and are not unique to this work.

Before proceeding with the governing equations, we introduce some more notations:

During swing, the robot configuration can be described by $\boldsymbol{\theta} = [\theta_{ns}, \theta_s]^T$ with θ_{ns} and θ_s the angles made respectively by the non-support (swing) and the support leg with the vertical (counterclockwise positive). The state vector $\boldsymbol{q}$ associated with the robot is then:

$$\boldsymbol{q} = [\boldsymbol{\theta}, \dot{\boldsymbol{\theta}}]^T = [\theta_{ns}, \theta_s, \dot{\theta}_{ns}, \dot{\theta}_s]^T \tag{2.1}$$

During transition, since both legs are in contact with the ground, the robot configuration can be completely described by the half inter-leg angle α, or equivalently by the step length L, defined as the distance between robot feet. α and L are related by $L = 2l \sin \alpha$, as shown in Fig. 2.2.

As the robot walks, the forward component of velocity of its center of mass changes continuously (as in human locomotion) . Therefore we introduce the term *average speed of progression* (ASP) of the robot, denoted as v, in order to quantify its forward movement averaged over the cycle. In case of a 2^n-periodic gait, v is a constant. When $n = 0$ (i.e., 1-periodic gait), v is expressed as $\frac{L}{T}$, with T the step period. For larger values of n, v is the value of $\frac{L_k}{T_k}$ (with k a step counter) averaged over 2^n consecutive steps, see Fig. 2.2. The calculation of v gets impossible for a chaotic gait. We have then to be content with only an "average" ASP.

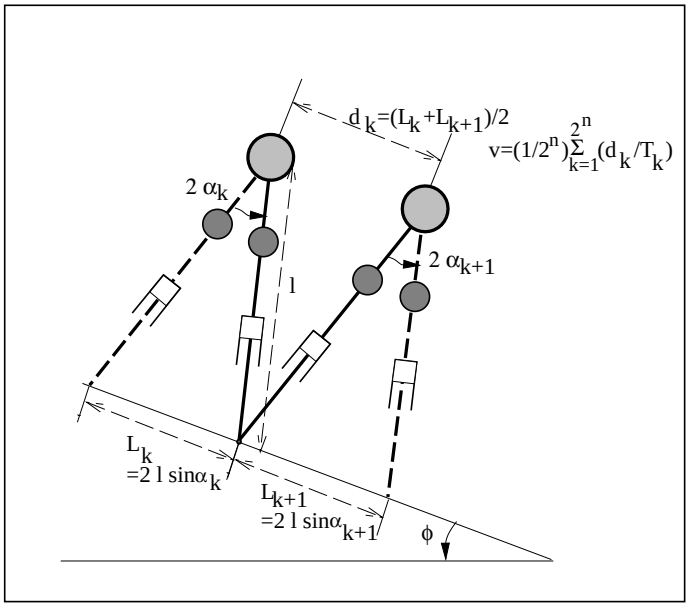

Figure 2.2: Model of a compass-like biped robot walking down a slope.
Transition stage (the subscript $_k$ is the step counter).

2.3 The governing equations

2.3.1 Dynamics of the swing stage

The dynamic equations of the swing stage are similar to the well-known double-pendulum equations. Since the legs of the robot are assumed identical, the equations are similar regardless of the support leg considered. They have the following form:

$$\boldsymbol{M}(\boldsymbol{\theta})\ddot{\boldsymbol{\theta}} + \boldsymbol{N}(\boldsymbol{\theta},\dot{\boldsymbol{\theta}})\dot{\boldsymbol{\theta}} + \boldsymbol{g}(\boldsymbol{\theta}) \;=\; \mathbf{0} \tag{2.2}$$

where $\boldsymbol{M}(\boldsymbol{\theta})$ is the 2×2 inertia matrix, symmetric positive definite, $\boldsymbol{N}(\boldsymbol{\theta},\dot{\boldsymbol{\theta}})$ is a 2×2 matrix with the centrifugal terms, and $\boldsymbol{g}(\boldsymbol{\theta})$ is a 2×1 vector of gravitational torques. The details of the Eqs. (2.2), and the expressions for $\boldsymbol{M}(\boldsymbol{\theta})$, $\boldsymbol{N}(\boldsymbol{\theta},\dot{\boldsymbol{\theta}})$ and $\boldsymbol{g}(\boldsymbol{\theta})$ can be found in Appendix A.1 (Eqs. (A.8), (A.9) and (A.10)).

Using (2.1), Eqs. (2.2) can also be written in the state-space form:

$$\dot{\boldsymbol{q}} = \frac{d}{d\,t}\begin{pmatrix} \boldsymbol{\theta} \\ \dot{\boldsymbol{\theta}} \end{pmatrix} = \begin{pmatrix} \dot{\boldsymbol{\theta}} \\ -\boldsymbol{M}^{-1}(\boldsymbol{\theta})\left[\boldsymbol{N}(\boldsymbol{\theta},\dot{\boldsymbol{\theta}})\dot{\boldsymbol{\theta}} + \boldsymbol{g}(\boldsymbol{\theta})\right] \end{pmatrix} \tag{2.3}$$

Since no dissipation takes place during swing, the total mechanical energy E of the robot is conserved during this stage.

2.3.2 Transition equations

Equations of the transition stage follow immediately from the collision assumptions A6-A7, page 14:

- Assumption A6, page 14 leads to:

$$\boldsymbol{\theta}^+ = \boldsymbol{J}\boldsymbol{\theta}^- \tag{2.4}$$

  with:

$$\boldsymbol{J} = \begin{pmatrix} 0 & 1 \\ 1 & 0 \end{pmatrix} \tag{2.5}$$

  The matrix $\boldsymbol{J}$ exchanges the support and the swing leg angles for the upcoming swing stage. The pre-impact and post-impact variables are identified respectively with the superscripts - and +.

- With the assumption A7 we can linearly relate the post-impact and pre-impact angular velocities of the robot:

$$\dot{\boldsymbol{\theta}}^+ \quad = \quad \boldsymbol{H}(\alpha)\dot{\boldsymbol{\theta}}^- \tag{2.6}$$

  The computation of the matrix $\boldsymbol{H}$ is provided in Appendix A.3 (Equations (A.35), (A.36) and (A.37)).

Eqs. (2.4) and (2.6) can be written together as:

$$\boldsymbol{q}^+ = \boldsymbol{W}(\alpha)\boldsymbol{q}^- \tag{2.7}$$

with:

$$\boldsymbol{W}(\alpha) = \begin{pmatrix} \boldsymbol{J} & 0 \\ 0 & \boldsymbol{H}(\alpha) \end{pmatrix} \tag{2.8}$$

Moreover, it follows from the robot geometry that during transition:

$$\theta_{ns}^- + \theta_s^- = -2\phi \qquad (\text{or } \theta_{ns}^+ + \theta_s^+ = -2\phi \text{ using (2.4)}) \tag{2.9}$$

$$\theta_{ns}^- - \theta_s^- = 2\alpha \qquad (\text{or } \theta_s^+ - \theta_{ns}^+ = 2\alpha \text{ using (2.4)}) \tag{2.10}$$

The assumption that the angular momentum of the robot is conserved during transition does not explicitly indicate how the mechanical energy of the robot changes during this stage. From physical considerations, it is expected that it does not increase. In fact, in Appendix B, we explicitly calculate the change in mechanical energy through the transition stage, denoted ΔE, and prove that it is always negative. Although this does not guarantee that our model is correct, we are at least assured that it is realistic.

2.4 Normalized expressions

As is true in general, it is significantly more advantageous to study the robot dynamics by means of normalized parameters. A remarkable property of the equations of our biped robot is that they can be normalized with respect to mass and length variables:

Property 2.1

- *The swing stage Eqs. (2.2) can also be written as:*

$$\boldsymbol{M}_n(\boldsymbol{\theta})\ddot{\boldsymbol{\theta}} + \boldsymbol{N}_n(\boldsymbol{\theta},\dot{\boldsymbol{\theta}})\dot{\boldsymbol{\theta}} + \frac{1}{a}\boldsymbol{g}_n(\boldsymbol{\theta}) = 0 \tag{2.11}$$

  with $\boldsymbol{M}_n(\boldsymbol{\theta})$, $\boldsymbol{N}_n(\boldsymbol{\theta},\dot{\boldsymbol{\theta}})$ and $\boldsymbol{g}_n(\boldsymbol{\theta})$ depending not on m, m_H, a and b, but only on μ and β.

- *Transition Eqs. (2.7) are already normalized, since the matrix $\boldsymbol{W}(\alpha)$ does not depend on m, m_H, a and b, but only on the dimensionless ratios μ and β.*

Appendix A.4 details the normalization process, see Eqs. (A.39), (A.40) and (A.41).

The following two properties are the direct consequences of Property 2.1. They are of key importance for the forthcoming Section 4, since they establish that a comprehensive analysis of passive compass gait with respect to its internal parameters m, m_H, a and b can be performed by considering only the dimensionless ratios μ and β:

Property 2.2

Gait characteristics of a robot with arbitrary masses m and m_H can always be deduced from those of a robot whose masses are in the same proportion, for instance m'

and $m_H\frac{m'}{m}$*, with* m' *an arbitrary value. More precisely, let us introduce the scalar* k_m *as:*

$$k_m = \frac{m}{m'} \tag{2.12}$$

Then, the passive gait characteristics of the two above-mentioned compass robots satisfy:

Compass with masses m' *and* $m_H\frac{m'}{m}$	*Compass with masses* m *and* m_H
$\boldsymbol{q}$, α, L, T, v	$\boldsymbol{q}$, α, L, T, v
E, ΔE	$k_m E$, $k_m \Delta E$

Passive gait analysis can therefore be achieved by varying only the mass ratio μ*.*

Property 2.3

Passive gait characteristics for a compass robot with arbitrary lengths a *and* b *can always be deduced from those of a compass whose lengths are in the same proportion, for instance* a' *and* $b\frac{a'}{a}$*, with* a' *an arbitrary value. More precisely, let us introduce the scalar* k_a *as:*

$$k_a = \frac{a}{a'} \tag{2.13}$$

Then, the passive gait characteristics of the two above-mentioned robots satisfy:

Compass with lengths a' *and* $b\frac{a'}{a}$	*Compass with lengths* a *and* b
$\boldsymbol{\theta}$	$\boldsymbol{\theta}$
$\dot{\boldsymbol{\theta}}$	$\frac{1}{\sqrt{k_a}}\dot{\boldsymbol{\theta}}$
α	α
L	$k_a L$
T	$\sqrt{k_a}T$
v	$\sqrt{k_a}v$
E	$k_a E$
ΔE	$k_a \Delta E$

Passive gait analysis can therefore be achieved by varying only the length ratio β*.*

The proofs of Properties 2.2 and 2.3 are provided in Appendix A.4.

3 Characteristics of steady passive compass gaits

Simulation trials reveal that the passive compass gait robot can walk down a slope with a steady gait. A thorough analysis of this behavior is presented in Section 4. This section consists of a first insight of the passive gaits. In Section 3.1, we describe a typical symmetric gait, using the phase diagram of the robot to identify the important time instants in a walk cycle. Next, in Section 3.2, we study in detail the interchange of the kinetic and potential energies of the robot as it characterizes its motion. Then, in Section 3.3, we explore quantitatively the contraction of phase space volumes in the neighborhood of a symmetric gait. Finally, in Section 3.4, we explore the stability of the linear and the nonlinear model of the robot around a periodic solution.

3.1 Description of a typical steady passive gait

Let us discuss the characteristics of a steady passive compass gait with the help of a phase portrait of the robot. There are several existing definitions of the phase space and phase portrait in the literature [BPV84], [Hil94]. The two most popular definitions describe the phase space as the space consisting of the generalized coordinate/generalized momentum variables or the generalized coordinate/generalized velocity variables. For our purpose we find it useful and physically more comprehensible to adopt the latter definition. According to this definition the phase space is identical to the state space.

The phase space of the compass gait robot is 4-dimensional. Since we cannot graphically visualize this high dimensional space we limit ourselves to a 2D projection of the robot's phase portrait. This reduced portrait involves the displacement and the velocity of only one leg. Fig. 3.1 shows such a phase portrait of the robot after it has walked sufficiently long such that the initial transients have died down and the robot has settled down to a periodic gait. The leg considered alternately becomes the support leg and the swing leg. As expected, a cyclic phase trajectory is observed in the figure. Since this is a symmetric gait, the phase portrait associated with the other leg would be exactly identical. The phase portraits associated with more complex gaits, such as an 8-periodic gait or a chaotic gait are slightly different from Fig. 3.1 as will be seen in Section 4.2.4 (Figs. C.30 and C.36).

In Fig. 3.1 we may start following the phase trajectory at the instant marked I corresponding to time $t = 0^+$, when the rear leg just loses contact with the ground (i.e., it becomes the swing leg). The corresponding stick diagram shows a black

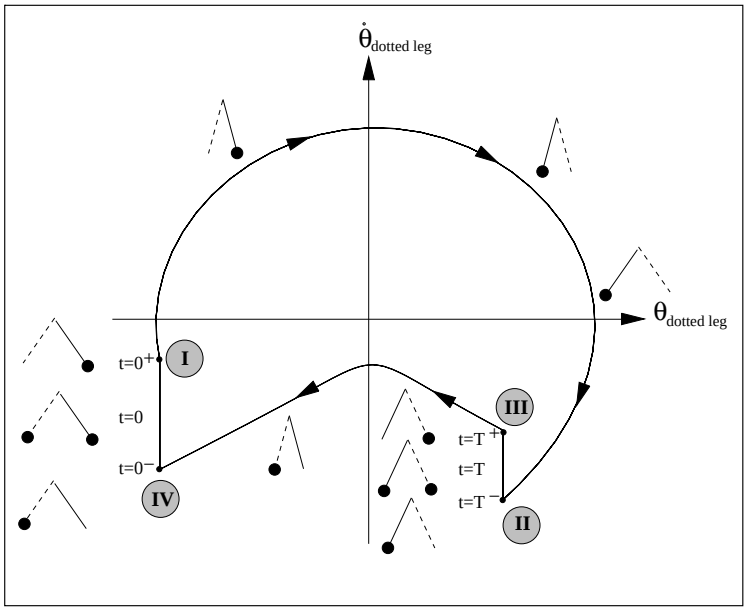

Figure 3.1: Phase portrait of a symmetric walk. This figure corresponds to only one leg of the biped, the actual phase of the system being higher dimensional. One cycle in the figure corresponds to two steps of the robot. In the figure we have indicated some of the time stamps important in the dynamic evolution of the biped. On the outside of the cyclic portrait, the configuration of the biped has been shown with small stick diagrams. In these diagrams, one leg is dotted, the other leg is solid, and a black dot at the foot indicates the supporting leg.

dot on the front foot to imply ground contact. The phase trajectory evolves in the clockwise sense in this diagram as shown by the arrowheads. While crossing the velocity axis (at a positive velocity), the biped is in the vertical configuration. Instant II corresponds to time $t = T^-$ when the swing leg is about to touch the ground. The impact between the swing foot and the ground occurs at $t = T$. We observe a velocity jump II$\rightarrow$III due to this impact. The upper half of the cycle (I$\rightarrow$II) depicts the swing leg suspended as a simple pendulum from a moving point (hip). At instant III ($t = T^+$), the swing leg becomes the support leg and executes the lower half of the phase plane diagram (II$\rightarrow$III). This half of the phase portrait corresponds to the motion of the support leg "hinged" at the point of support as an inverted simple pendulum. The velocity jump of the current leg (the non-support

leg of instant I) observed between IV and I is due to the impact of the other leg with the ground.

As mentioned before, Fig. 3.1 is a 2D projection of the complete 4D phase space. A projection of the phase space does not necessarily preserve the properties of the original phase portrait of a system. For example if we construct a 2D phase diagram of our robot before it settles down to a periodic gait we can see phase trajectories crossing each other. Crossing of two or more trajectories in the phase space of an autonomous system is impossible since that would imply that the same initial condition (the intersection point of the trajectories) can give rise to two different evolutions of the system which is un-physical. Also, the adjacency of two trajectories in a phase space projection does not necessarily imply their adjacency in the actual phase space; trajectories of equal length at two different parts of the diagrams do not necessarily imply their equality since in the higher dimensional space they may be inclined at different angles to our point of view. Some features are, however, preserved in the projection of a phase space, a very useful one being the fact that cycles in the full phase space are also cycles (possibly self-intersecting) in its projections.

3.2 The energy balance in a steady passive gait

We have learned that a passive biped, when started with favorable initial conditions, may walk down an inclined plane in a steady periodic gait. We associate this to a *limit cycle* behavior of the nonlinear system represented by Eqs. (2.3) and (2.7).

A limit cycle is a periodic solution of a system and is represented by a closed loop in the phase space [Hil94]. The difference between a simple periodic solution and a limit cycle is that the latter exerts its influence in its neighborhood. An attracting limit cycle pulls and absorbs all neighboring trajectories towards itself, the neighborhood region in which this pull is in effect is called the *basin of attraction* of the limit cycle. An attracting limit cycle is also called a *stable* limit cycle since small perturbations in the states of a system lying on the limit cycle reduces to zero in the long run. A stable limit cycle is an *attractor* of the system. One can similarly have a repelling or unstable limit cycle which amplifies all small perturbations around it. Finally a saddle limit cycle has both attracting and repelling features.

Typically, the existence of a stable limit cycle in a dynamical system is associated with a contraction of the phase space volume as the system evolves in time. The presence of a dissipative element in the system causes such phase space volume contractions and favors (but does not guarantee in any way) the existence of a

stable limit cycle. Noting that our robot has a phase space volume conserving Hamiltonian dynamics during the swing stage, we naturally search for the cause of the existence of limit cycle. The answer lies in the impact equations (Eq. 2.6). In fact, the robot behaves similar to that of a mechanical clock. In a clock the energy loss due to friction during a cycle is exactly compensated by an energy "kick" at definite intervals. For the robot the kinetic energy (K) gain due to the conversion of gravitational potential energy (P) in a step is absorbed in an instantaneous impact at the touchdown. Thus we see that there is, in effect, a feedback type of mechanism governing the system.

Significant amount of insight may be gained from a K vs. P plot as shown in Fig, 3.2. Since the mechanical energy $E = K + P$ is conserved during swing stage, the energy trajectory line is a straight line (line BC) making a 135° angle with the K axis. The trajectory of the robot, starting from point A follows ABAC. Point C is the touchdown point where an impact occurs with the ground. The instantaneous loss of K is shown by the line CD in the diagram. Total loss of P in one step is given by the distance AD = CF. For a periodic gait therefore, CF = CD.

For a symmetric steady gait of the robot on a plane of known inclination, the amount of P lost in each step can be calculated:

$$P_I - P_{II} = P_{III} - P_{IV} = \Delta P = m_C g L sin\phi \tag{3.1}$$

A relationship between the angular velocities of the legs at the beginning of the swing can be derived from (3.1): since for a symmetric gait a left step (I→III) and a right step (III→I) are identical, we have:

$$\boldsymbol{\theta}_{III} = \boldsymbol{\theta}_I \tag{3.2}$$

$$\dot{\boldsymbol{\theta}}_{III} = \dot{\boldsymbol{\theta}}_I \tag{3.3}$$

As the mechanical energy E of the robot is constant during the swing phase, we have $E_I = E_{II}$, where $E_I = P_I + K_I$ and $E_{II} = P_{II} + K_{II}$. From these we get,

$$K_{II} - K_I = P_I - P_{II} \tag{3.4}$$

All steps being identical, we have $K_{III} = K_I$. We then obtain from Eq. (3.4) that

$$K_{II} - K_{III} = P_I - P_{II} \tag{3.5}$$

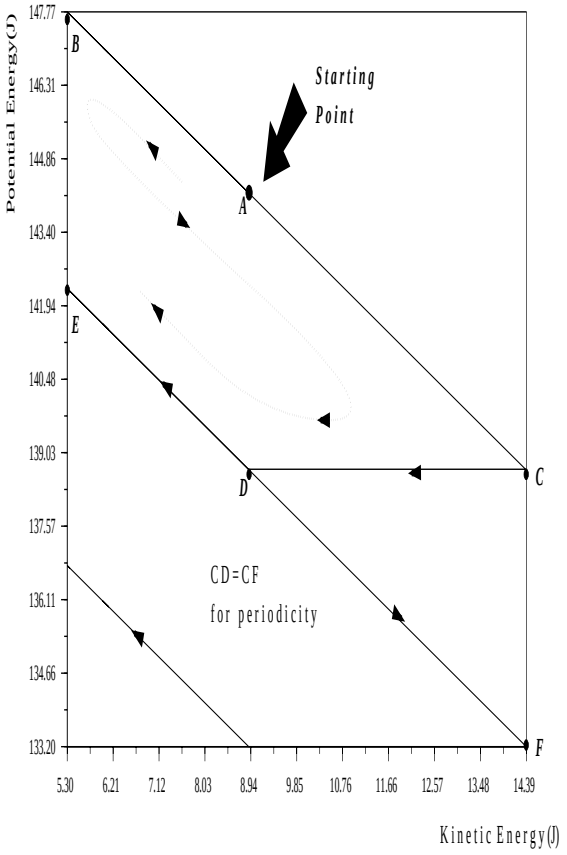

Figure 3.2: The K vs P diagram of a compass gait. For a steady symmetric gait CD = CF.

Using (2.6) and (3.3) we write:

$$\dot{\boldsymbol{\theta}}_{II} = \boldsymbol{H}^{-1}\dot{\boldsymbol{\theta}}_{I}, \tag{3.6}$$

Writing out in full Eq. (3.5) and using (3.1), we get:

$$\frac{1}{2}\left[\dot{\boldsymbol{\theta}}_{II}{}^{T}\boldsymbol{M}_{II}\dot{\boldsymbol{\theta}}_{II} - \dot{\boldsymbol{\theta}}_{III}{}^{T}\boldsymbol{M}_{III}\dot{\boldsymbol{\theta}}_{III}\right] = m_C g L sin\phi \tag{3.7}$$

Moreover, since the robot configuration is constant during the transition, $\boldsymbol{M}_{II} = \boldsymbol{M}_{III}$. Finally, using Eqs. (3.3) and (3.6), $\dot{\boldsymbol{\theta}}_{II}$ and $\dot{\boldsymbol{\theta}}_{III}$ can be expressed in terms of $\dot{\boldsymbol{\theta}}_I$. Therefore, we get:

$$(\boldsymbol{H}^{-1}\dot{\boldsymbol{\theta}}_I)^T \boldsymbol{M}_{II}(\boldsymbol{H}^{-1}\dot{\boldsymbol{\theta}}_I) - (\dot{\boldsymbol{\theta}}_I)^T \boldsymbol{M}_{II}(\dot{\boldsymbol{\theta}}_I) = 2m_C gLsin\phi. \tag{3.8}$$

On simplification, this becomes,

$$\dot{\boldsymbol{\theta}}_I{}^T((\boldsymbol{H})^{-1T}\boldsymbol{M}_{II}\boldsymbol{H}^{-1} - \boldsymbol{M}_{II})\dot{\boldsymbol{\theta}}_I = 2m_C gLsin\phi. \tag{3.9}$$

The last equation is in terms of the two velocity variables of the robot. If there exists a symmetric gait of step length L on a certain slope ϕ the equation gives us the relationship that must exist between the two velocity variables at the beginning of the swing stage. In other words, if we are somehow able to determine one of the velocities, the other velocity may be calculated. This equation does not help us in establishing the existence of a limit cycle in the system but rather checks the validity of a cycle once it has been identified. The information that we used in obtaining the equation is based on energy alone and does not involve the dynamics of the system in between two touchdowns. The latter would have required the integration of the nonlinear equations.

3.3 Contraction of phase space volumes

The contraction of phase space volumes evoked in the previous section is quantitatively investigated in this section.

During the swing stage the robot dynamics is Hamiltonian and the phase space volumes are conserved. Since the robot behavior confirms the presence of a stable limit cycle and since a stable limit cycle is necessarily accompanied by a contraction of phase space volumes, we focus on the behavior of the robot during the transition stage.

Let $\boldsymbol{q}^{*^-}$ be the state vector of the robot in a symmetric gait just before the transition[1]. We consider a parallelepiped with edge vectors $\varepsilon_j \boldsymbol{i}_{j,\ j\in\{1,\ldots,4\}}$, with ε_j small scalars and $\boldsymbol{i}_j$ the j^{th} column of identity matrix $\boldsymbol{I}_4$, starting from the vertex $\boldsymbol{q}^{*^-}$ and denote it by $\mathcal{P}^-$. We calculate here the change in the volume of this parallelepiped (i.e., the "volume" of the ensemble of states just before collision) due

[1] nevertheless, the following analysis equally applies for the case when the state vector q^{*^-} lies on a limit cycle of a 2^n-periodic gait or on a strange attractor, if the gait is chaotic

to transition. When $\boldsymbol{q}^{*-}$ is perturbed by an amount $\delta\boldsymbol{q}^-$, a first order approximation of the state vector just after transition is (Eq. (2.7)):

$$\boldsymbol{q}^{*+} + \delta\boldsymbol{q}^+ = \boldsymbol{W}(\alpha^*)(\boldsymbol{q}^{*-} + \delta\boldsymbol{q}^-) + \left.\frac{\partial \boldsymbol{W}(\alpha)\boldsymbol{q}^{*-}}{\partial\alpha}\right|_{\alpha=\alpha^*} .\delta\alpha \tag{3.10}$$

Using (2.10), Eq. (3.10) can be written in a compact form as:

$$\delta\boldsymbol{q}^+ = \boldsymbol{W}_1(\boldsymbol{q}^{*-})\delta\boldsymbol{q}^- \tag{3.11}$$

with:

$$\boldsymbol{W}_1(\boldsymbol{q}^{*-}) = \begin{pmatrix} \boldsymbol{J} & \boldsymbol{0} \\ \left.\frac{\partial \boldsymbol{H}(\frac{1}{2}(\theta_{ns}^- - \theta_s^-))\dot{\boldsymbol{\theta}}^{*-}}{\partial\boldsymbol{\theta}^-}\right|_{\boldsymbol{\theta}^-=\boldsymbol{\theta}^{*-}} & \boldsymbol{H}(\alpha^*) \end{pmatrix} \tag{3.12}$$

In view of Eq. (3.12), a first-order approximation of the "image" of $\mathcal{P}^-$ through transition is the polyhedra $\mathcal{P}^+$ whose edge vectors starting from $\boldsymbol{q}^{*+}$ are $\varepsilon_j \boldsymbol{w}_{1,j}$, $j\in\{1,\ldots,4\}$, where $\boldsymbol{w}_{1,j}$ is the j^{th} column of matrix $\boldsymbol{W}_1(\boldsymbol{q}^{*-})$. Since the volume of a n-dimensional parallelepiped is given by the determinant of the matrix whose columns are the n edge vectors starting from a same vertex, [Hec94], volumes of $\mathcal{P}^-$ and $\mathcal{P}^+$ are respectively:

$$\text{volume}(\mathcal{P}^-) = \left|\prod_{j=1}^{4} \varepsilon_j\right| \qquad \text{volume}(\mathcal{P}^+) = \left|\left(\prod_{j=1}^{4} \varepsilon_j\right).\det(\boldsymbol{W}_1(\boldsymbol{q}^{*-}))\right| \tag{3.13}$$

Therefore a first-order approximation of the change in volume in the phase space during the transition stage of a steady gait is, using (3.12) and (3.13):

$$\frac{\text{Volume}^+}{\text{Volume}^-} = |\det(\boldsymbol{H}(\alpha^*))| \tag{3.14}$$

The determinant can be computed from Eqs. (A.35), (A.36) and (A.37):

$$\begin{aligned} \det(\boldsymbol{H}(\alpha^*)) &= \frac{\det(\boldsymbol{Q}^-(\alpha^*))}{\det(\boldsymbol{Q}^-(\alpha^*))} \\ &= \frac{m^2a^2b^2}{-m^2a^2b^2 - mm_Hb^2l^2 - m^2b^2l^2(1-\cos^2(2\alpha^*))} \end{aligned} \tag{3.15}$$

Since the physical values of the mass and the lengths as well as the quantity $1-cos^2(2\alpha)$ are always positive in the Eq. (3.15), the denominator of this equation is

always negative. In other words, the absolute value of $\det(\boldsymbol{H}(\alpha^*))$ is clearly inferior to 1 which indicates that phase space volumes are always contracted. This was expected since the transition stage is dissipative, see Appendix B. It is important to remember that contraction does not imply stability. For example, the volume of a parallelepiped all of whose sides except one are contracted by a factor of two during each transition, while the last side is doubled, will vanish eventually. However the parallelepiped consists of diverging points and will not represent a stable gait. The local stability of the compass gait is however demonstrated in the following Section 3.4. The rate of contraction describes how fast the neighboring trajectories converge. For the robot model considered in Section 4.2.1 i.e., $\mu = 2$ and $\beta = 1$, $\det(\boldsymbol{H}(\alpha^*)) \approx 0.1$. Thus we can say that locally the phase space volumes are contracted by a factor of 10 indicating that the limit cycles (or the strange attractors for chaotic gaits) are highly attractive.

3.4 Study of gait stability

3.4.1 Definition of gait stability

The concept of gait stability as applied to a walking machine is hard to define but is crucial for the performance analysis of the system. The conventional definitions of stability of a system in the sense of Lyapunov (around an equilibrium point) are not immediately suitable for such systems. If $\boldsymbol{q}(t)$ is a periodic solution of a pure autonomous robot, $\boldsymbol{q}(t+\delta)$ is another solution, for every value of δ. Periodic solutions of an autonomous system cannot be asymptotically stable in the usual way. Therefore, we define below the stability of a system in terms of its *orbital stability.*

As in [HM86], it is natural to say that a gait is stable if, *starting from a steady closed phase trajectory, any finite disturbance leads to another nearby trajectory of similar shape.* Furthermore, if in spite of the disturbance, the system returns to the original cycle, the gait is called asymptotically stable.

Adapting from [Hay85] we can present the notion of orbital stability in a more mathematical framework. Let us consider a continuous nonlinear system of the general form

$$\dot{\boldsymbol{q}} = \boldsymbol{f}(\boldsymbol{q}, t). \tag{3.16}$$

We may eliminate time t from this equation and express the solution as a trajectory in the vector space of the states $\boldsymbol{q}$. In this reduced space one may imagine time to be the velocity associated with the representative point along the trajectory. The

phase trajectory C of Eq. (3.16) is said orbitally stable if, *given* $\varepsilon > 0$, *there is* $\delta > 0$ *such that, if* R' *is a representative point (on another trajectory* C'*) which is within a distance* δ *of* C *at time* t_0*, then* R' *remains within a distance* ε *of* C *for* $t \geq 0$. If no such δ exists, C is orbitally unstable. Analogous to the asymptotic stability of the conventional definition we may say that if the trajectory C is orbitally stable and, in addition, the distance between R' and C tends to zero as time goes to infinity, the trajectory C is asymptotically orbitally stable.

The following remarks qualify this definition:

- Orbital stability requires that the trajectories C and C' remain near each other, whereas Lyapunov stability of the solution $\boldsymbol{q}(t)$ requires that, in addition, the representative points R and R' (on C and C' respectively) should remain close to each other, if they were close to each other initially.

- Orbital stability does not take into account the adjacency of a slightly perturbed trajectory as a function of time. In Fig. 3.3 we see two spiral trajectories of a certain 1-dimensional system in its extended phase space (with position, velocity, *and* time). The two trajectories are the time evolutions from two nearby initial conditions. Although the time evolution of the trajectories are very different (they move away from each other), they belong to the same limit cycle orbit in the phase space which, in this case, is a unit circle. Thus the system will be called orbitally stable (around the limit cycle) but not stable in the sense of Lyapunov.

We have presented the nature of a stable limit cycle in the phase plane of one joint variable of the biped. As shown in the schematic representation in Fig. 3.4, the effect of a stable limit cycle in the phase plane will be to attract and absorb the nearby phase trajectories. A system starting from a state on the limit cycle will continue to travel on it. The shaded area in the figure indicates the region in which this attracting feature is valid. This shaded area is termed the *domain* or the *basin of attraction* of the limit cycle. It is interesting to note that the whole phase plane can be the basin of attraction of a limit cycle. For a certain selection of its parameters the Van der Pol oscillator exhibits this characteristic.

Finally, let us emphasize that the orbital stability of the limit cycle in Fig. 3.1 does not require that any of the two halves of the complete cycle (the half I$\rightarrow$III and the half III$\rightarrow$I) be itself a part of a closed limit cycle. In fact, the presence of a limit cycle in a differential-algebraic hybrid system such as our biped robot does not at all imply any periodic behavior in the differential part or the algebraic part

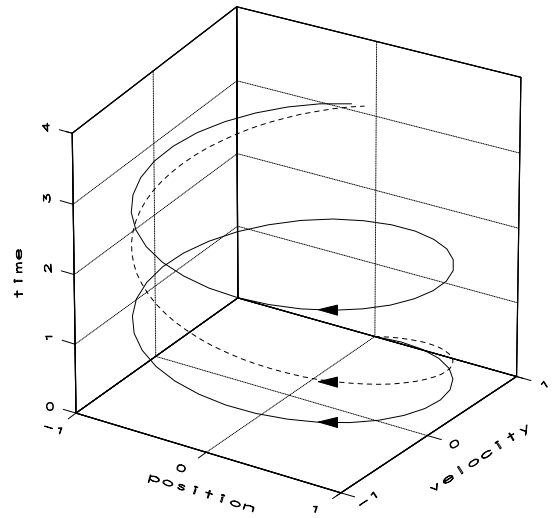

Figure 3.3: The figure shows two trajectories (one solid and one dashed) which are orbitally identical although they go farther and farther away from each other in time. The orbital signatures of both the trajectories is a unit circle.

of the equations. This is important for understanding the behavior of such hybrid systems. As a simple example of a hybrid system let us consider a ball bouncing on the ground. If the ball/ground impact is perfectly elastic the ball will conserve its mechanical energy and will continue to bounce indefinitely. This periodic behavior is the combined outcome of the differential motion equation as well as the impact equation of the ball. We do not see any periodic behavior if we look, for example, only at the differential part of the system which states that the downward acceleration of the ball is equal to the acceleration due to gravity. Mathematical definition and analysis of the stability of systems with impacts may be found in [GR87].

3.4.2 Linearized model – an exact solution

The only equilibrium of the compass biped is $\boldsymbol{q}_e = \mathbf{0}$ (both legs vertical with zero angular velocities). Linearization of the swing Eqs. (2.3) around $\boldsymbol{q}_e$ produces state equations of the form:

$$\dot{\boldsymbol{q}} = \boldsymbol{A}\boldsymbol{q} \tag{3.17}$$

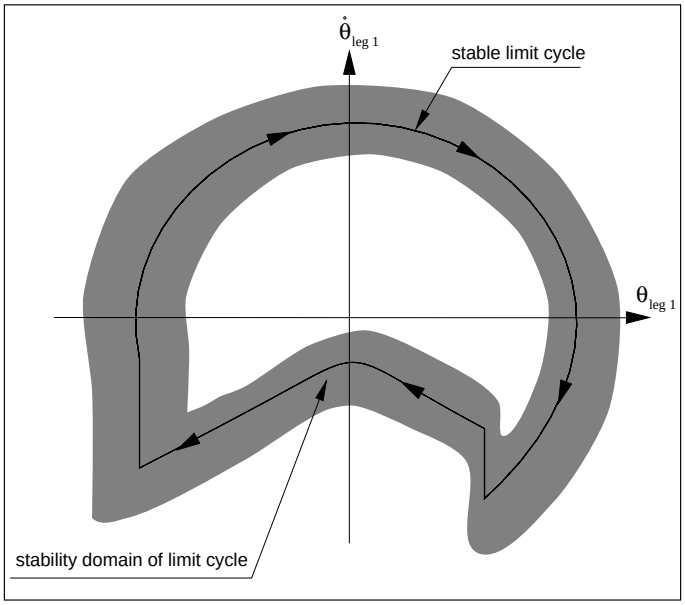

Figure 3.4: Stable periodic walk. The effect of a stable limit cycle in the phase plane will be to attract and absorb the nearby phase trajectories. If the system starts from a certain state on the limit cycle, it will continue to travel on it. The shaded area shows the stable domain of the limit cycle.

The computation of the matrix $\boldsymbol{A}$ is provided in Appendix A.2 (Eq. (A.17)).

Explicit integration of Eqs. (3.17) is straightforward. It is therefore relatively simple to investigate the existence and the stability of symmetric passive gaits for the linearized model.

Existence of symmetric gait The existence of a symmetric gait can be studied from basic algebraic computations. The time-evolution of the state vector $\boldsymbol{q}$ from the initial conditions $\boldsymbol{q}_0$ is given by the explicit integration of Eq. (3.17) as:

$$\boldsymbol{q}(t) = e^{\boldsymbol{A}\,t}\boldsymbol{q}_0 \tag{3.18}$$

Let T denote the instant when the non-support leg touches the ground. The state vector $\boldsymbol{q}$ at the end of the swing is expressed as:

$$\boldsymbol{q}(T^-) = e^{\boldsymbol{A}\,T}\boldsymbol{q}_0 \tag{3.19}$$

whereas at the beginning of the following swing, it is, using (2.7) and (3.19):

$$\boldsymbol{q}(T^+) = \boldsymbol{D}(\alpha, T)\boldsymbol{q}_0 \tag{3.20}$$

where the matrix $\boldsymbol{D}$, called the *step-to-step matrix* [McG90], is given by:

$$\boldsymbol{D}(\alpha, T) = \boldsymbol{W}(\alpha)e^{\boldsymbol{A}T} \tag{3.21}$$

Therefore, the linearized robot model may exhibit a symmetric gait *if and only if there exist couples* (α^*, T^*) *such that* $\boldsymbol{D}(\alpha^*, T^*)$ *possesses at least one unity eigenvalue.* If this condition is satisfied, then the state at the beginning of the swing stage of the symmetric gait, termed $\boldsymbol{q}^*$, is given by the eigenvector of $\boldsymbol{D}(\alpha^*, T^*)$ associated with the unity eigenvalue and such that (Eq. (2.10)):

$$\theta_s^* - \theta_{ns}^* = 2\alpha^* \tag{3.22}$$

The slope ϕ^* corresponding to this symmetric gait is (Eq. (2.9)):

$$\phi^* = -\frac{1}{2}(\theta_{ns}^* + \theta_s^*) \tag{3.23}$$

A careful numerical analysis of the eigenvalues of matrix $\boldsymbol{D}(\alpha, T)$ reveals that, *for a given slope* ϕ*, there exist many couples* (α^*, T^*)*, i.e., several possible symmetric gaits.* For each slope ϕ, only two of these gaits look "natural" in the sense that their swing stage consists of a single forward swing of the non-support leg before it hits the ground. On the contrary, the swing stage of the other gaits consists of several back and forth swings of the non-support leg before it hits the ground. The major difference between the two natural gaits, as will be shown below, is that one is stable and the other unstable.

A remarkable feature of these gaits is that the step period T^* of these natural and unnatural gaits depends very little on the slope ϕ. On the contrary, the other characteristic features of the steady gaits, such as the touchdown velocity, are sensitive to the value of the ground slope.

Local stability We follow [GH83] in defining the *first return map* or the *Poincaré map* of a dynamic system:

For a dynamic system represented in the form of Eq. (3.16) the function $\boldsymbol{f} : U \to \mathcal{R}^n$ is called a *vector field* that generates a *flow* $\phi_t : U \to \mathcal{R}^n$. Let us take a

local cross-section $\Sigma \subset \mathcal{R}^n$ of dimension $n-1$ of a periodic orbit γ of the flow ϕ_t. The hypersurface Σ is chosen such that it is always transverse to the flow. Next we denote by p the unique point where γ intersects with Σ and by $V \subseteq \Sigma$ some neighborhood of p. The *Poincaré map* $P : V \to \Sigma$ is defined for a point $q \in V$ by $P(q) = \phi_\tau(q)$ where $\tau = \tau(q)$ is the time taken for the orbit $\phi_t(q)$ based at q to return for the first time to Σ. The time to return, τ, depends upon q and is not necessarily equal to the period of the trajectory γ.

One way to investigate the local orbital stability of the limit cycles obtained above for the linearized robot model consists in slightly perturbing the states from the limit cycles and then observing the Poincaré map. As a natural choice of the Poincaré Section, we take the instant when the swing leg of the robot leaves the ground.

Let T_k denote the step period of the k^{th} step and $\boldsymbol{q}_k$ the state vector at the beginning of the k^{th} swing. In view of (3.20), $\boldsymbol{q}_k$ is the solution of the following discrete system:

$$\boldsymbol{q}_{k+1} = \boldsymbol{D}(\alpha_{k+1}, T_k)\boldsymbol{q}_k \tag{3.24}$$

Eq. (3.24) is clearly the Poincaré map. It is also called the step-to-step equations [McG90] [Fra96]). With respect to the Eq. (3.16), a *fixed point* of the function $\boldsymbol{f}$ corresponds to equilibria or stationary solutions. A fixed point of a Poincaré map corresponds to a periodic trajectory of the dynamic equations of the system. The state vector $\boldsymbol{q}^*$ of a symmetric gait is then a fixed point of the Eqs. (3.24):

$$\boldsymbol{q}^* = \boldsymbol{D}(\alpha^*, T^*)\boldsymbol{q}^* \tag{3.25}$$

Let us perturb $\boldsymbol{q}^*$ and investigate the propagation of the perturbation. A small perturbation $\delta\boldsymbol{q}_k$ at step k manifests itself as a deviation $\delta\boldsymbol{q}_{k+1}$ at step $k+1$, while satisfying Eq. (3.24):

$$\boldsymbol{q}^* + \delta\boldsymbol{q}_{k+1} = \boldsymbol{D}(\alpha^* + \delta\alpha_{k+1}, T^* + \delta T_k)(\boldsymbol{q}^* + \delta\boldsymbol{q}_k) \tag{3.26}$$

Linearizing Eqs. (3.26) around $\boldsymbol{q}^*$, we have:

$$\boldsymbol{q}^* + \delta\boldsymbol{q}_{k+1} = \boldsymbol{D}(\alpha^*, T^*)(\boldsymbol{q}^* + \delta\boldsymbol{q}_k) + \left.\frac{\partial \boldsymbol{D}(\alpha, T^*)\boldsymbol{q}^*}{\partial \alpha}\right|_{\alpha=\alpha^*} .\delta\alpha + \left.\frac{\partial \boldsymbol{D}(\alpha^*, T)\boldsymbol{q}^*}{\partial T}\right|_{T=T^*} .\delta T \tag{3.27}$$

Using (3.25), Eq. (3.27) can be simplified as:

$$\delta\boldsymbol{q}_{k+1} = \boldsymbol{D}(\alpha^*, T^*)\delta\boldsymbol{q}_k + \left.\frac{\partial \boldsymbol{D}(\alpha, T^*)\boldsymbol{q}^*}{\partial \alpha}\right|_{\alpha=\alpha^*} .\delta\alpha + \left.\frac{\partial \boldsymbol{D}(\alpha^*, T)\boldsymbol{q}^*}{\partial T}\right|_{T=T^*} .\delta T \tag{3.28}$$

In addition, $\delta \boldsymbol{q}_k$ satisfies the following pair of equations (following from (2.9)-(2.10)):

$$\theta^*_{s,k} + \delta\theta_{s,k} + \theta^*_{ns,k} + \delta\theta_{ns,k} = -2\phi^* \quad (3.29)$$

$$\theta^*_{s,k} + \delta\theta_{s,k} - \theta^*_{ns,k} - \delta\theta_{ns,k} = 2(\alpha^* + \delta\alpha_k) \quad (3.30)$$

which, in view of (3.22) and (3.23), can be simplified as:

$$\delta\theta_{s,k} + \delta\theta_{ns,k} = 0 \quad (3.31)$$

$$\frac{1}{2}\boldsymbol{\lambda}\delta\boldsymbol{\theta}_k = \delta\alpha_k \quad (3.32)$$

with $\boldsymbol{\lambda} = [\,-1 \quad 1]$. $\delta\theta_{ns,k}$ and $\delta\theta_{s,k}$ are clearly not independent, for any k integer (Eq.3.31). Redundancy in the Eqs. (3.28) can be eliminated by considering only $\delta\alpha_k$, instead of $\delta\theta_{ns,k}$ and $\delta\theta_{s,k}$ (using (3.32)). Conversely, $\delta\boldsymbol{\theta}_k$ can be computed from $\delta\alpha_k$ as (using (3.31) and (3.32)):

$$\delta\boldsymbol{\theta}_k = \boldsymbol{\lambda}\delta\alpha_k \quad (3.33)$$

Let us finally divide $\boldsymbol{D}$ into 2×2 submatrices:

$$\boldsymbol{D}(\alpha, T) = \begin{pmatrix} \boldsymbol{D}_{11}(\alpha, T) & \boldsymbol{D}_{12}(\alpha, T) \\ \boldsymbol{D}_{21}(\alpha, T) & \boldsymbol{D}_{22}(\alpha, T) \end{pmatrix} \quad (3.34)$$

Using (3.33) and (3.34), Eq. (3.28) can then be written in a compact form as:

$$\begin{pmatrix} \delta\alpha_{k+1} \\ \delta\dot{\boldsymbol{\theta}}_{k+1} \\ \delta T_k \end{pmatrix} = \boldsymbol{K} \begin{pmatrix} \delta\alpha_k \\ \delta\dot{\boldsymbol{\theta}}_k \end{pmatrix} \quad (3.35)$$

with:

$$\boldsymbol{K} = \boldsymbol{K}_1^{-1}\boldsymbol{K}_2 \quad (3.36)$$

$$\boldsymbol{K}_1 = \begin{pmatrix} \boldsymbol{\lambda} & \boldsymbol{0}_2 & -\frac{\partial(\boldsymbol{D}_{11}(\alpha^*,T)\boldsymbol{\theta}^* + \boldsymbol{D}_{12}(\alpha^*,T)\dot{\boldsymbol{\theta}}^*)}{\partial T}\Big|_{T=T^*} \\ -\frac{\partial(\boldsymbol{D}_{21}(\alpha,T^*)\boldsymbol{\theta}^* + \boldsymbol{D}_{22}(\alpha,T^*)\dot{\boldsymbol{\theta}}^*)}{\partial \alpha}\Big|_{\alpha=\alpha^*} & \boldsymbol{I}_2 & -\frac{\partial(\boldsymbol{D}_{21}(\alpha^*,T)\boldsymbol{\theta}^* + \boldsymbol{D}_{22}(\alpha^*,T)\dot{\boldsymbol{\theta}}^*)}{\partial T}\Big|_{T=T^*} \end{pmatrix} \quad (3.37)$$

$$\boldsymbol{K}_2 = \begin{pmatrix} \boldsymbol{D}_{11}(\alpha^*, T^*)\boldsymbol{\lambda} & \boldsymbol{D}_{12}(\alpha^*, T^*) \\ \boldsymbol{D}_{21}(\alpha^*, T^*)\boldsymbol{\lambda} & \boldsymbol{D}_{22}(\alpha^*, T^*) \end{pmatrix} \quad (3.38)$$

In view of (3.35), *the passive symmetric gait* $\boldsymbol{q}^*$ *is stable if the eigenvalues of the upper* 3×3 *block of the matrix* $\boldsymbol{K}$ *are inside the unit circle* (the stability of the

last equation, involving δT_k, is subordinated to the stability of the others). Let us however emphasize that this result comes from two successive linearizations – the linearization of the swing equations (from (2.3) to (3.17)) and the linearization of the step-to-step equations (from (3.24) to (3.35)) and therefore is valid only locally around $\boldsymbol{q}^*$.

As for the linearized compass gait model, only one of the "natural" symmetric gaits is stable. When the initial conditions $\boldsymbol{q}_0$ for the linearized robot model are chosen equal to the unstable one, two distinct behaviors are observed, depending on the value of the slope ϕ. For small slope, the system remains on the unstable steady gait for some step, and then converges to the stable one. On the contrary, for higher slopes, the unstable steady gait does not belong any longer to the basin of attraction of the stable one, the robot collapses after few steps. The limit slope between these two behaviors depends on the values of parameters m, m_H, a and b.

As for the unnatural 1-periodic steady gaits, they are very unstable: when $\boldsymbol{q}_0$ is chosen equal to the state vector $\boldsymbol{q}^*$ of such steady gaits, the robot collapses very quickly.

3.4.3 Local stability of the nonlinear limit cycles

When considering the original nonlinear dynamic equations of the robot, the existence and the stability of passive gaits can no longer be investigated via analytical methods.

The existence and the characteristics of steady passive compass gaits are addressed in Section 4 using numerical simulations. Their stability can be addressed by using exactly the same methodology as that proposed in Section 3.4.2 for the linearized model of the robot, but we have to rely upon numerical simulations.

Let us again choose as the Poincaré section the instant when the swing leg leaves the ground. The Poincaré map is denoted below as $\boldsymbol{F}$:

$$\boldsymbol{q}_k = \boldsymbol{F}(\boldsymbol{q}_{k-1}) \tag{3.39}$$

For a small perturbation $\delta\boldsymbol{q}^*$ around the limit cycle the nonlinear mapping function $\boldsymbol{F}$ can be expressed in terms of Taylor series expansion as

$$\boldsymbol{F}(\boldsymbol{q}^* + \delta\boldsymbol{q}^*) \approx \boldsymbol{F}(\boldsymbol{q}^*) + (\nabla\boldsymbol{F})\delta\boldsymbol{q}^* \tag{3.40}$$

where $\nabla\boldsymbol{F}$ is the gradient of $\boldsymbol{F}$ with respect to the state variables. Since $\boldsymbol{q}^*$ is a fixed point of the mapping, we can rewrite Eq. (3.40) as

$$\boldsymbol{F}(\boldsymbol{q}^* + \delta\boldsymbol{q}^*) \approx \boldsymbol{q}^* + (\nabla\boldsymbol{F})\delta\boldsymbol{q}^* \tag{3.41}$$

The mapping $\boldsymbol{F}$ is stable if the Poincaré map of a perturbed state is closer to the fixed point. This property can be viewed as the contraction of the phase space around the limit cycle. Mathematically this means that the magnitude of the eigenvalues of $\nabla \boldsymbol{F}$ at the fixed point $\boldsymbol{q}^*$ are strictly less than one. From Eq. (3.41) we write $(\nabla \boldsymbol{F})\delta \boldsymbol{q}^* \approx \boldsymbol{F}(\boldsymbol{q}^* + \delta \boldsymbol{q}^*) - \boldsymbol{q}^*$ where $\boldsymbol{F}(\boldsymbol{q}^* + \delta \boldsymbol{q}^*)$ is the Poincaré map of the perturbed state $\boldsymbol{q}^* + \delta \boldsymbol{q}^*$. As it is not practical to analytically calculate the matrix $(\nabla \boldsymbol{F})$ we have to proceed numerically. One straightforward method is to perturb one state at a time by a small amount and observe its Poincaré map. Repeating this procedure at least four times (once for each of the four states) we obtain an equation of the form

$$(\nabla \boldsymbol{F})\boldsymbol{\Upsilon} = \boldsymbol{\Omega} \tag{3.42}$$

where the 4×4 diagonal matrix $\boldsymbol{\Upsilon}$ contains as its diagonal entries the perturbations of the state variables $(\delta {q_i}^*)$. The i^{th} column of the 4×4 matrix $\boldsymbol{\Omega}$ gives, in terms of the four states, how far away from the periodic solution the Poincaré map shows up due to a perturbation of the i^{th} state variable. Assuming that $\boldsymbol{\Upsilon}$ is non-singular, the computation of $\nabla \boldsymbol{F}$ is straightforward: $\nabla \boldsymbol{F} = \boldsymbol{\Omega}\boldsymbol{\Upsilon}^{-1}$.

As an example, we have derived the value of $\nabla \boldsymbol{F}$ for a compass robot whose masses and lengths are $m = 5$ Kg, $m_H = 10$ Kg and $a = b = 0.5$ meter, walking with a steady passive gait on a 3^o downward incline. We have obtained:

$$\nabla \boldsymbol{F} = \begin{bmatrix} -0.439 & -0.500 & -0.003 & -0.169 \\ 0.439 & 0.500 & 0.003 & 0.169 \\ 0.147 & -2.933 & 0.082 & -1.065 \\ -0.877 & -1.846 & 0.011 & -0.633 \end{bmatrix} \tag{3.43}$$

An immediate calculation shows that the eigenvalues of $\nabla \boldsymbol{F}$ are:

$$\begin{array}{c} -0.252 + 0.215i \\ -0.252 - 0.215i \\ 2.554\,10^{-9} \\ 0.014 \end{array} \tag{3.44}$$

Their absolute values are 0.332, 0.332, $2.554\,10^{-9}$, and 0.014. Thus the cycle is stable. There is a zero eigenvalue. This is expected ([Ott93]). The existence of this eigenvalue can be interpreted as that the perturbation has been along the limit cycle and the resulting trajectory corresponding to this perturbation is along the same limit cycle.

The fact that the steady gait was found by means of numerical simulations practically guarantees that the limit cycle is stable. Unless we *accidentally* hit the exact states on an unstable limit cycle, it will never be encountered in numerical trials.

4 Influence of robot parameters on steady passive gaits

The biped robot equations consist of nonlinear ordinary differential equations (for the swing stage) and algebraic equations (for the transition). To our knowledge, there is no analytical method for studying the limit cycles of such a hybrid system. Therefore, we present in this section a thorough numerical analysis of these equations. All simulation results presented in this report were obtained by *Scilab-2.2* software [Sci96].

In order to study the effect of some of the pertinent quantities that affect the robot gait characteristics we differentiate between the *parameters* and the *gait descriptors*. In the rest of this text, by a parameter we will refer to a quantity which can be directly altered. The ground slope ϕ is a first obvious parameter. In view of Properties 2.2 and 2.3, a comprehensive analysis of passive compass gait can be performed by considering only 2 others parameters, namely the dimensionless ratios μ and β. A gait descriptor, on the other hand, will refer to the observed (measurable or computable) quantities which may not be modified directly but are indirectly influenced by the parameters. The gait descriptor that appear the most meaningful to us are the state variables $\boldsymbol{q}$, the half inter-leg angle at touchdown α, the step-period T, the average speed of progression v, the total mechanical energy of the robot E and the change in mechanical energy δE due to impact.

In Section 4.1, we question the validity of the linearized compass model which was introduced in Section 3.4.2. In Section 4.2 we present and discuss the results of the systematic numerical analysis of the nonlinear model of the compass gait.

4.1 Validity of the linear approximation

One of the most important information about the robot dynamics, from both the practical and theoretical points of view, is the expanse of the basin of attraction of the stable limit cycle. If the *initial conditions*, i.e., the starting states of the robot, are within the basin of attraction, it will eventually converge to the limit cycle. The shape and size of the basin of attraction of a limit cycle is in general a function of the robot parameters and are not amenable to direct analytical calculations. In order

to "guess" the initial conditions within the attraction basin boundary of the limit cycle corresponding to a stable passive gait we use the initial conditions calculated from the analytical solution of the linearized robot model. If the robot were truly a linear system these initial conditions would have been precisely on the limit cycle. We observe, in general, that for small ϕ and small β the initial conditions obtained from the linear model lie within the attraction basin. μ has no effect on this.

Often the initial guess corresponding to the linear model fails to converge the robot to a limit cycle. In these cases we chose as the initial conditions, the state vector $\boldsymbol{q}$ corresponding to a known steady gait of a robot whose parameters (ϕ, μ, β) are close to those of the robot under study. We succeed in this way to characterize steady gait out of the domain of validity of the linear approximation.

The domain of validity of the linear approximation, i.e., the range of values of parameters ϕ, β and μ for which our initializing method is successful, can be precised as follows. We have considered:

- a first set of robots whose mass ratio μ is 2 (i.e., $m = 5$ Kg and $m_H = 10$ Kg) and whose length ratio β varies from 0.1 to 10 (l remaining equal to 1 meter),
- a second set of robots whose length ratio β is 1 (i.e., $a = b = 0.5$ meter) and whose mass ratio μ varies from 0.1 to 10 (m_C remaining equal to 20 Kg).

We have simulated these two sets of robots on four slopes: $\phi = 0.25^o$, $\phi = 1.5^o$, $\phi = 3^o$ and $\phi = 4^o$, with $\boldsymbol{q}_0$ always chosen equal to the stable symmetric gait computed for the linearized model of the robot. We have observed that in these cases the robot actually converges to the steady gait,

for	$\beta < 4.8$	when	$\phi = 0.25^o$	and	$\mu = 2$
for	$\beta < 2.9$	when	$\phi = 1.5^o$	and	$\mu = 2$
for	$\beta < 1.5$	when	$\phi = 3^o$	and	$\mu = 2$
for	$\beta < 1$	when	$\phi = 4^o$	and	$\mu = 2$
for any	μ	when	$\phi = 0.25^o$	and	$\beta = 1$
for any	μ	when	$\phi = 1.5^o$	and	$\beta = 1$
for any	μ	when	$\phi = 3^o$	and	$\beta = 1$

No steady gait was found for $\phi = 4^o$ and $\beta = 1$. An interesting result was noted when $\phi = 1.5^o$, $\mu = 2$ and $2.5 \leq \beta < 2.9$. Starting from the $\boldsymbol{q}_0$ corresponding to that of the stable 1-periodic steady gait of the linearized robot model, the actual nonlinear robot model converges to a 2-periodic steady gait.

In order to compare the steady gaits of the nonlinear robot model and its linearized version, numerical simulations have been run for μ and β respectively set to 2 and 1, and slope ϕ gradually increasing from 0.25^o to 3.75^o.

It is not unexpected that for higher slopes the difference between the original and the linearized models of the biped will be more pronounced. For higher slopes the robot's dynamics involve larger joint angles and higher velocities and thus the validity of the linear approximation (which assumes $\boldsymbol{q} = \mathbf{0}$) diminishes. If we compare the gait descriptors of the nonlinear model to those of the linearized version on the same slope we interestingly find that the sensitivity of the descriptors to the linearization vary widely. Referring to Figs. 4.2, 4.3, and 4.4 we see that:

- gait descriptors related to the *angular position*, i.e., $\boldsymbol{\theta}$, α and L are less sensitive to the linearization. $\boldsymbol{\theta} - \boldsymbol{\theta}_l$, $\alpha - \alpha_l$ and $L - L_l$ vary from 0.14 % to 0.4 % depending on the value of ϕ.
- the touchdown joint velocities $\dot{\boldsymbol{\theta}}$ are more sensitive. $\dot{\boldsymbol{\theta}} - \dot{\boldsymbol{\theta}}_l$ varies from 0.15 % to 9 % depending on the value of ϕ. The mechanical energies $E = K + P$ vary up to 18 % depending on the slope (since E depends on $\dot{\boldsymbol{\theta}}^2$). We have the same result for the ratio $\frac{\Delta E}{E}$ since ΔE depends mainly on L (Eq. (3.1)).
- the step periods vary from 2.3 % to 11%. The same result holds for the ASP v (as expected in view of its definition, page 15)

Finally we have tried, without success, to identify more than one stable steady gaits for a given slope. Since this result is not analytic we cannot claim it as a proof. If each slope is indeed associated with one single gait of the robot that would indicate to the existence of an underlying organizing principle which automatically determines all the independent motion descriptors (such as the step length L, the step period T,...) once the ground slope ϕ is specified.

4.2 Numerical simulations of the nonlinear model

In the following three sections we systematically study the effect of the evolution of the gait descriptors as a function of its parameters. As mentioned earlier, the three parameters considered are the ground slope ϕ (Section 4.2.1), the mass ratio μ (Section 4.2.2) and the length ratio β (Section 4.2.3). For higher values of all of these parameters the robot exhibits *period doubling* phenomena. As the parameters are gradually increased successive period doublings in the form of *flip bifurcations*

[TS91] modify the robot gait from a symmetric gait to a series of asymmetric 2^n-periodic gaits with progressively higher values of n. For sufficiently higher values of the parameters the gait becomes chaotic. The phenomena of bifurcation and chaos are treated with special emphasis in the Section 4.2.4.

4.2.1 Effect of slope

In order to investigate the effect of ground slope ϕ on the robot gait we have set $\mu = 2$ and $\beta = 1$, and increased ϕ from 0.25^o to 5^o in steps of 0.25^o. It was then increased by 0.01^o up to 5.2^o in order to analyze 4-periodic, 8-periodic and chaotic steady gaits. For the robot considered in this set of numerical simulations, symmetric gait are observed up to $\phi = 4.37^o$.

The evolution of the gait descriptors T, α, $\dot{\theta}_s$, v, E and $\frac{\Delta E}{E}$ as functions of ϕ are presented in the Figs. C.4 to C.9. These diagrams are called *bifurcation diagrams* [GH83] [Hil94] [BPV84]. A bifurcation diagram typically depicts the evolution of a gait descriptor (the step length of a biped robot, for example) as a function of a parameter (the ground slope in this case). A point in the parameter space where a bifurcation occurs is called the *bifurcation point*. The dotted line starting from the first bifurcation point in the Figs. C.4 to C.9 denotes the arithmetic average of all the solution values of the descriptors under study. The chaotic gaits, represented in the bifurcations diagrams by a continuous distribution of points, are shown exclusively on Figs. C.4, C.5 and C.10[2]. Fig. C.9 depicts 4 limit cycles corresponding to 4 different values of ϕ.

Bifurcation and chaos will be discussed in greater detail in Section 4.2.4. We focus here on symmetric gaits. It is worth-mentioning that all of the gait descriptors evolve monotonically during symmetric gaits. This reinforces our earlier finding that a given ground slope *uniquely* defines a robot gait with all of its descriptors. This property is exploited in [EG94], [GEK96] and [GKE96] in formulating a control strategy for the robots. It was shown that a scalar control law which seeks to converge the mechanical energy of the "actively controlled" robot to that corresponding to a known passive gait ensures, interestingly, the convergence of *all* the state variables of the robot.

Figure C.10 shows the dependence of the *step ratio* of the robot gait on the slope. Step ratio is defined as the step length divided by the step frequency [Koo89]. The reason that we have considered the behavior of this gait descriptor is that it is known

[2] They have been omitted in all other bifurcation diagrams, including those of Sections 4.2.2 and 4.2.3 for the sake of clarity

to be reasonably constant over a wide range of walking velocities and for different subjects. For normal walking the step ratio ranges from 0.39 to 0.44 m-s for men and from 0.34 to 0.40 m-s for women.

We make two further comments regarding the effect of slope on the general behavior of the compass robot. The first is that the robot takes longer and faster steps as the slope is increased. This behavior can be observed in Fig. C.11 where the limit cycles are seen being enlarged along both the position and the velocity axes when ϕ is raised. Second, the kinetic energy K of the robot increases with ϕ. This is expected as K is roughly proportional to $\|\dot{\boldsymbol{\theta}}\|^2$. Fig. C.9 shows that the ratio $\frac{\Delta E}{E}$ also increases with higher slopes.

4.2.2 Effect of mass ratio

In this set of simulations $\beta = 1$, and 4 different ground slopes of $\phi = 0.25^o$, 1.5^o, 3^o and 4^o have been considered. Mass ratio μ was increased from 0.1 to 1 in steps of 0.1 and from 1 to 10 in steps of 1.

Figs. C.12 to C.17 present the evolution of the same 6 gait descriptors, T, α, $\dot{\theta}_s$, v, E and $\frac{\Delta E}{E}$, as functions of μ (using a logarithmic axis), and Fig. C.18 depicts 3 limit cycles corresponding to 3 different values of μ.

In Fig. C.11 we had noticed that as ϕ increased the maximum angular velocity attained by the robot and its touchdown inter-leg angle increased as well. From the limit cycles in Fig. C.18 we observe that for higher μ the touchdown inter-leg angle (thus the step length) increases but its maximum joint velocity decreases. This is manifested by the progressively "flatter" limit cycles. The average speed of progression however increases monotonically for higher values of μ.

The step period of the robot increases with higher μ. The robot exhibits a flip bifurcation for the 4^o slope when $\mu = 4$. For weaker slopes no bifurcation is observed for $\mu \leq 10$.

Mechanical energy E of the robot increases when the value of μ is increased, see Fig. C.16. An increase in μ is equivalent to a transfer of mass from the legs to the hip, i.e., an elevation of the robot's center of gravity. The potential energy of the robot is thus increased with higher μ. The variation of the kinetic energy is difficult to explain since on one hand the average velocity of the robot increases along with μ and, on the other hand, the maximum angular velocity of the robot decreases. In any case, the mechanical energy increases with μ.

Unlike the other descriptors, $\dot{\theta}_s$ and $\frac{\Delta E}{E}$ do not change monotonically with μ. As shown in Fig. C.14 and C.17 respectively, the $\dot{\theta}_s$ vs μ curves show a distinct minimum for each slope whereas the $\frac{\Delta E}{E}$ vs μ curves show a maximum.

4.2.3 Effect of length ratio

In this set of simulations $\mu = 2$, and 4 different ground slopes, $\phi = 0.25°$, $1.5°$, $3°$ and $4°$ have been considered. For each slope we increased β from 0.1 in steps of 0.1 until the gait becomes chaotic. The value of β at which the gait becomes chaotic depends on the value of the slope.

Figs. C.19 to C.24 present the evolution of the 6 gait descriptors as functions of β (using a logarithmic axis). Fig. C.25 depicts 3 limit cycles corresponding to 3 different values of β.

For each of the ground slopes considered an increase in β causes period doubling cascades. Steeper is the slope, lower is the value of β leading to the first period doubling. We observe that the

symmetric (i.e., 1-periodic) gait turns 2-periodic	for $\beta = 3.5$	when $\phi = 0.25°$
	for $\beta = 2.5$	when $\phi = 1.5°$
	for $\beta = 1.7$	when $\phi = 3°$
	for $\beta = 1.2$	when $\phi = 4°$

The gait descriptors T, α, and $\frac{\Delta E}{E}$ monotonically increase with β (Figs. C.19, C.20 and C.24). The descriptors $\dot{\theta}_s$ (in absolute value), v and E on the other hand are monotonically decreasing (Figs. C.21, C.22 and C.23).

The following observations can be made from the figures. When β is increased, the robot exhibits longer and slower steps. Mechanical energy E of the robot decreases when β is raised. This is expected. Since the average velocity as well as $\|\dot{\boldsymbol{\theta}}\|$ decrease with increasing β, the kinetic energy of the robot should decrease. Moreover since a higher β corresponds to a lowering of the position of the leg center of mass, the potential energy should decrease also. Fig. C.24 shows that $\frac{\Delta E}{E}$ increases with an increase in β.

As seen in Fig. C.25 when β is increased, phase plane limit cycles are slightly enlarged along the position axis, indicating longer steps, and contracted along the velocity axis, indicating that the robot slows down. In addition, in the case where β is small, i.e., mass center of the leg is near the hip the angular velocity of the support leg is almost constant during the swing.

4.2.4 Period doubling, bifurcation

In previous sections, it was pointed out that passive 1-periodic gaits turn 2^n-periodic when one or more of the parameters ϕ, μ and β increase. In the following we discuss

the occurrence of this period doubling phenomenon, also called a flip bifurcation, in the context of our compass-gait biped robot.

In order to introduce the period doubling phenomenon, let us consider a non-linear dynamical system whose Poincaré map is one-dimensional:

$$x_{k+1} = F(x_k) \tag{4.1}$$

If this dynamical system exhibits a stable limit cycle, then the mapping F possesses one stable fixed point x^*. This situation is depicted in Fig. 1(a): for any initial condition x_0 (except $x_0 = 0$ or $x_0 = 1$, which are unstable fixed points), the system converges to the stable limit cycle represented by x^* in the Poincaré section. x^* is the intersection of the Poincaré map with the 45° line.

Let us now continuously modify one parameter (such as the inertia, damping etc.) of the system under consideration. The mapping F is then clearly altered, and its stable fixed point x^* may either shift or become unstable. The instability of a fixed point, typically called a *structural instability*, results in a completely different behavior of the dynamical system. Fig. 1(b) describes one possible structural instability: x^* has become an unstable fixed point. Any initial condition different from $x_0 = 0$, $x_0 = 1$ and $x_0 = x^*$ converges now to a limit cycle crossing the Poincaré section alternately at x_1^* and x_2^*, since these 2 points are related by:

$$\begin{array}{rcl} x_2^* & = & F(x_1^*) \\ x_1^* & = & F(x_2^*) \end{array} \tag{4.2}$$

Since the period of the stable limit cycle has doubled, this structural instability is generally termed as a period doubling [BPV84], [Hil94], or a flip bifurcation [TS91].

Dynamical systems whose Poincaré maps are higher dimensional may also experience flip bifurcations. When the considered parameter has a value less than that corresponding to the bifurcation point the system exhibits a stable limit cycle. In this case all the eigenvalues of the Jacobian of the Poincaré map in the neighborhood of the limit cycle are within the unit circle. Modifying the parameter alters the eigenvalues, and at bifurcation point at least one crosses the unit circle. The particular fashion in which an eigenvalue crosses the unit circle determines the type of structural instability that the system undergoes. Flip bifurcation corresponds to an eigenvalue leaving the unit circle along the real axis, with a negative real part. Fig. C.26 presents the evolution of the eigenvalues of the Jacobian of the compass

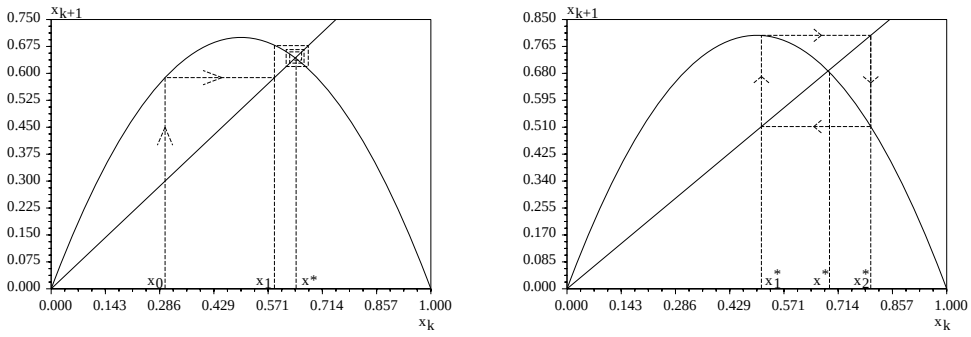

(a) 1-periodic behavior (b) 2-periodic behavior

Figure 4.1: Example of a Poincaré map experimenting period doubling.

Poincaré map as a function of ϕ. All are real, and one of them actually reaches the value -1 when the first bifurcation point is reached at $\phi = 4.37^o$.

The 2-periodic limit cycle generated by a period-doubling may experience a further period-doubling, giving rise to a 4-periodic limit cycle. This phenomenon, repeated ad infinitum, is called *a period doubling cascade* and is recognized as one of the possible routes leading to chaos. Occurrences of period doubling for various sets of robot parameters are listed in Table 1. Regardless of the parameter considered, we observe that the successive period doublings occur after progressively smaller intervals of parameter variation. Starting from the 1-periodic gait it is relatively easy to detect the bifurcations since the range of variation of the parameters from one bifurcation to the next are relatively large. The subsequent bifurcations are more sensitive to the parameter variation and a relatively small change in the parameter value may cause several bifurcations which are difficult to segregate individually. This is expected in view of general results on period doubling cascades [BPV84].

Such period doubling cascades leading to chaotic behavior have already been observed for passive planar hopping robots which possess a smaller dimension than that of the compass. 2^n-periodic gaits were observed in hopping robots [Rai86] (they were termed "limping gaits"), and analyzed in [VB90], [MB91], [OB93] and [Fra96] [KB91].

In Fig. C.27 we detail the behavior of the compass robot during a period doubling cascade ensuing from the parameter ϕ (other parameters are kept constant, $\mu =$

Parameters	1-periodic	2-periodic	4-periodic	
$\mu = 2, \beta = 1$	$0.25^o \leq \phi < 4.5^o$	$4.5^o \leq \phi < 5^o$	$5^o \leq \phi < 5.02^o$	...
$\phi = 0.25^o, \beta = 1$	$0.1 \leq \mu < 10$	-	-	...
$\phi = 1.5^o, \beta = 1$	$0.1 \leq \mu < 10$	-	-	...
$\phi = 3^o, \beta = 1$	$0.1 \leq \mu < 10$	-	-	...
$\phi = 4^o, \beta = 1$	$0.1 \leq \mu < 4$	$4 \leq \mu < 4$	-	...
$\phi = 0.25^o, \mu = 2$	$0.1 \leq \beta < 3.5$	$3.5 \leq \beta < 8.6$	not observed	...
$\phi = 1.5^o, \mu = 2$	$0.1 \leq \beta < 2.5$	$2.5 \leq \beta < 2.9$	$2.9 \leq \beta < 3$	...
$\phi = 3^o, \mu = 2$	$0.1 \leq \beta < 1.7$	$1.7 \leq \beta < 1.9$	$1.9 \leq \beta < 2$	...
$\phi = 4^o, \mu = 2$	$0.1 \leq \beta < 1.2$	$1.2 \leq \beta < 1.4$	$1.4 \leq \beta < 1.5$	...

Parameters		8-periodic	16-periodic
$\mu = 2, \beta = 1$	...	$5.02^o \leq \phi < 5.04^o$	not observed
$\phi = 0.25^o, \beta = 1$	...	-	-
$\phi = 1.5^o, \beta = 1$	...	-	-
$\phi = 3^o, \beta = 1$	...	-	-
$\phi = 4^o, \beta = 1$	...	-	-
$\phi = 0.25^o, \mu = 2$	...	-	-
$\phi = 1.5^o, \mu = 2$	...	not observed	$3 \leq \beta < 3.1$
$\phi = 3^o, \mu = 2$	...	$2 \leq \beta < 2.1$	not observed
$\phi = 4^o, \mu = 2$	...	not observed	-

Table 1: Occurrences of period doubling

$2, \beta = 1$). The figure plots the k^{th} vs. $k + 1^{th}$ angular positions of the swing leg at the beginning of the stage, i.e., it consists of only one component of compass Poincaré map. For a 1-periodic robot gait θ_{ns} is the same in every cycle. This gait is therefore represented by a point on the first bisector line. As we change the ground slope, the representative point moves along the bisector line from the right-hand top corner of Fig. C.27, as indicated by the arrow.

The first period doubling occurs when $\phi = 4.37°$. The compass gait turns 2-periodic and is therefore represented in Fig. C.27 by 2 points. Just after the first bifurcation the 2 representative points differ only slightly from the representative point of the 1-periodic gait from which they originate. The two steps are therefore very similar to the steps of the symmetric gait. Then, the two representative points move away from the first bisector line along the two branches shown by dotted lines in Fig. C.27. It follows that one step length is slightly longer and the other slightly

shorter than those of the corresponding symmetric gait. As we increase the slope the longer step is further elongated and the shorter step further shortened.

This continues until a second period doubling occurs when $\phi = 4.9°$. Each branch then gives rise to two sub-branches. The steps of the 4-periodic gait are strictly ordered. Their succession is as follows: a long step, a very short step, a very long step, a short step, and so on. The last clearly identifiable bifurcation occurs when $\phi = 5.01°$ as the robot gait becomes 8-periodic.

The period doubling cascade may also be observed using phase plane diagrams. A 1-periodic phase plane diagram was already shown in Fig. 3.1. Figs. C.28, C.29, C.30 present limit cycles for, respectively, 2-periodic, 4-periodic and 8-periodic gaits.

The phase plane limit cycle of a 1-periodic gait is a single-loop closed trajectory repeated after two robot steps. During one step the considered leg is in the swing stage and during the following one, it is in the support stage. Since the gait is symmetric, the robot legs are indistinguishable and the phase plane cycles of the two legs are identical.

In case of a 2-periodic gait, since all state descriptors are identical after every two steps, the phase plane limit cycle associated with one leg is still a single-loop closed trajectory repeated after two robot steps. The gait is however asymmetric, one leg always takes long steps, and the other always takes short steps. The limit cycles associated with the legs are therefore no longer identical.

In case of 2^n-periodic gaits, all the state variables repeat themselves after every 2^n steps. The phase plane diagram associated with one leg is therefore a 2^{n-1}-loop closed trajectory repeated after every 2^n steps, distinguishable from the phase plane diagram of the other leg. The visual inspection of the phase plane diagrams of the 4-periodic and the 8-periodic gait correctly indicates that they resulted from the bifurcation of respectively the preceding 2-periodic and the 4-periodic gaits.

For the asymmetric gait, some characteristic descriptors vary quite a lot from step to step, while others change little. For instance, in case of the 8-periodic gait shown in Fig. C.30, we have observed that:

the difference between maximum and average values of	E	equals	0.18 %
"	T	equals	8.62 %
"	α	equals	8.4 %
"	v	equals	15.7 %

4.2.5 Chaotic gaits

As mentioned previously, when $\mu = 2$, $\beta = 1$ and $\phi = 5.03°$, a 8-periodic gait is observed. If the parameter ϕ is further raised, several period doublings take place very quickly and starting from $\phi = 5.04°$ we are unable to detect any periodicity in the motion of the robot. Fig. C.31 provides 50 consecutive step periods of this steady gait. None are exactly equal. An order is however maintained: a long step period is always followed by a short one. Moreover, a histogram of the step periods, i.e., the frequency of occurrence of a small[3] range of step periods vs. the range, reveals 4 major clusters, Fig. C.32. This indicates that the gait is 2^n-periodic with a large n.

Steady gaits are still observed when ϕ is increased. Figs. C.33 and C.34 are the equivalents of Figs. C.31 and C.32 for $\phi = 5.2°$. This time, no clear order can be detected when considering 50 consecutive step periods, and we notice the presence of all the step periods within a range. Since *chaos* is qualitatively characterized by the unpredictability of system evolution and the presence of a "broad-band frequency" in the system power spectrum, we are allowed to qualify this steady gait as chaotic. Figs. C.35 and C.36 show the associated phase plane diagrams. The robot do not exhibit limit cycle behavior anymore but the trajectories stay on a *strange attractor* which is a manifold of a lower dimension in the phase space.

A Poincaré section of this strange attractor is presented in Fig. C.37. The hyperplane of section, $\theta_s = -2\phi - \theta_{ns}$, corresponds to the beginning of swing stages, see Eq. (2.9). Strange attractors of dynamic systems are generally known to possess a *fractal* or non-integer dimension. We can observe that the Poincaré section consists of multiple closed packed lines separated by empty spaces. The strange attractor is therefore neither a line nor a surface. It should thus have a dimension between 1 and 2. It is *not* an Euclidean entity.

The fractal dimension is defined as follows: let $n(\varepsilon)$ be the minimum number of hypercubes of length ε necessary to cover a set of points in an n-dimensional space. The fractal or Hausdorff-Besicovitch dimension of this set, denoted as D, is such that:

$$\lim_{\varepsilon \to 0} n(\varepsilon) = \varepsilon^{-D} \tag{4.3}$$

This definition is consistent with the usual definition of Euclidean dimension. A line segment of length d can be covered by $\frac{1}{\varepsilon}$ segments each of length εd. Using (4.3) we see that $D = 1$, as expected.

[3]The range is to be appropriately selected to be able to identify the four groups

The relationship (4.3) is however not very tractable when computing fractal dimensions in practice. An approximated dimension is therefore usually computed as follows. Let us choose m points $\boldsymbol{q}_i$ in the set whose dimension has to be determined, and then compute the values of the following function $n(r)$ for various r:

$$n(r) = \frac{1}{m^2}\Big(\text{number of pairs } i,j \ / \ \|\boldsymbol{q}_i - \boldsymbol{q}_j\| < r\Big) \tag{4.4}$$

Concretely, for a given point $\boldsymbol{q}_i$, we count the number of points $\boldsymbol{q}_{j,\,j\neq i}$ belonging to a hyper-sphere of radius r centered at $\boldsymbol{q}_i$. The same is done for all points and $n(r)$ is obtained in the end by summation. It can be understood as a kind of statistical approach. The approximated fractal dimension D_1 of the set is then such that:

$$\lim_{m\to\infty} n(r) = r^{D_1} \tag{4.5}$$

It can be shown, [BPV84], that D_1 bounds D from below.

Using (4.5), it can be computed that the fractal dimension of the strange attractor for our robot, whose Poincaré section is depicted in Fig. C.37, is 2.07. The attractor is thus dimensionally close to a Euclidean plane. This is a consequence of the strong phase space volume contraction observed in Section 3.3.

The "compact" structure of the strange attractor permits us to investigate it through some simplifications. Since the Poincaré section shown in Fig. C.37 is close to a line, most of the system behavior can be described using only one component of the Poincaré map, for instance $\theta_{ns,k+1} = f(\theta_{ns,k})$. This first return map has been plotted for increasing ϕ in Figs. C.38 to C.41. The first return map associated with the step period T has also been plotted for $\phi = 5.2^o$, Fig. C.42.

The establishment of the robot gait to the eventual chaotic regime is well depicted in Figs. C.38 to C.41. When $\phi = 5.03^o$, the gait is 8-periodic, it's first return map consists of 8 points as shown in Fig. C.27. When $\phi = 5.04^o$, the first return map consists of 8 distinguishable clusters of points. Through multiple period doubling bifurcations this 8-periodic gait gives rise to a 2^n-periodic gait with a large n. This gait still preserves some similarity with the 8-periodic gait from which it originates. For example, step order is still preserved since basic line drawings similar to the Figs. 4.1) prove that θ_{ns} always visits the 8 clusters in the same order, as indicated in Fig. C.38. We note that this order is that a large θ_{ns} (i.e., $|\theta_{ns}| > .4$ rad) is always followed by a small θ_{ns} (i.e., $|\theta_{ns}| < .4$ rad).

When $\phi = 5.08^o$, the 8 clusters of points merge into 2 larger packs. Some order is still preserved, since a large θ_{ns} is still always followed by a small one. The same

property still holds when $\phi = 5.12^o$, but in this case the first return map appears as a continuum of point. We are therefore very close to the "broad-band frequency" characteristic typical of chaotic behavior. Finally, when $\phi = 5.2$, we observe that predictability and periodicity have been completely destroyed, since a large θ_{ns} can be followed by another large one. The layered structure of the strange attractor can also be guessed from the first return map (it begins to appear for $\phi = 5.12^o$).

It is extremely interesting to note that that the first return maps of all of the robot gait descriptors look remarkably similar. For instance, the first return map of the step period T (Fig. C.42) looks like a rotated first return map of $\theta_{ns}(Fig.\ C.41)$. With this we can suggest that all the characteristics of the passive chaotic gait of our robot is somehow ensconced in the shape of its first return map, which can be viewed as a signature of the chaotic gait.

5 Conclusions and future work

We have studied the stability and the periodicity properties of the passive motion of a simple biped machine, the compass gait walker. We have observed that such a biped can walk down on an inclined plane in a steady and stable fashion. There is a strong indication that all the motion descriptors of such a gait is specified by only one parameter, for instance the slope of the inclined plane. The motion equations exhibit bifurcation phenomena at a certain slope angle: a 1-periodic motion changes to another stable periodic motion with unequal step lengths. On further increase in the slope angle the robot undergoes a period doubling cascade until its motion becomes chaotic. Bifurcation and chaos are also shown to be produced by changing the mass distribution of the robot.

It is instructive to remember that the difficulty in studying the behavior of this apparently simple biped mechanism is to a large part due to its hybrid differential-algebraic governing equations. The conditions for the existence of steady and stable limit cycles in the robot dynamics are dictated not only by the continuous differential equations but also by the algebraic switching conditions. This hybrid nature of the robot equations makes it especially difficult for us to employ the traditional nonlinear systems tools in our current study.

When analyzing the linearized compass model, unstable limit cycles have been observed. In order to identify such unstable behavior in compass nonlinear model, we would need to integrate the system back in time. Although not useful as a

viable "walk", these unstable limit cycles may tell us more about compass global properties.

We should remember that our system's behavior is influenced by our impact model which is not, by any means, the only available one. For the impact model to be of practical use, the robot gait should be robust against small parameter perturbations in the model. Such analysis has not been completed yet.

It would also be useful to be able to identify the boundary of the basin of attraction, i.e., the set of compass initial conditions from which this robot can walk in a steady fashion without any actuation. It would have been an interesting starting data before investigating the design of control laws for this system. Active compass gait is nevertheless discussed in our second research report dedicated to compass-like biped robot [GKE96].

Appendices

A Dynamic equations of the robot (in detail)

A.1 Swing stage equations

During the swing, the robot behaves like a planar double-pendulum (Assumption A4, page 14). Its dynamical equations can be derived using the well-known Euler-Lagrange approach:

$$\frac{d}{dt}\left(\frac{\partial\,\mathcal{L}(\boldsymbol{\theta},\dot{\boldsymbol{\theta}})}{\partial\dot{\boldsymbol{\theta}}}\right)-\frac{\partial\,\mathcal{L}(\boldsymbol{\theta},\dot{\boldsymbol{\theta}})}{\partial\boldsymbol{\theta}}=0 \tag{A.1}$$

where the Lagrangian $\mathcal{L}(\boldsymbol{\theta},\dot{\boldsymbol{\theta}})$ is the difference between the kinetic energy and the potential energy of the robot: $\mathcal{L}(\boldsymbol{\theta},\dot{\boldsymbol{\theta}})=K(\boldsymbol{\theta},\dot{\boldsymbol{\theta}})-P(\boldsymbol{\theta})$. The right-hand side term of (A.1) is 0, since the robot is completely passive.

In order to calculate the energy of the robot we simply consider the dynamics of the three distinct masses:

$$K(\boldsymbol{\theta},\dot{\boldsymbol{\theta}}) = \frac{1}{2}m_H\|\vec{\boldsymbol{v}}_H\|^2+\frac{1}{2}m\|\vec{\boldsymbol{v}}_s\|^2+\frac{1}{2}m\|\vec{\boldsymbol{v}}_{ns}\|^2 \tag{A.2}$$

$$P(\boldsymbol{\theta}) = m_H g l\cos\theta_s+mga\cos\theta_s+mg(l\cos\theta_s-b\cos\theta_{ns})+P_0 \tag{A.3}$$

where $\vec{\boldsymbol{v}}_H$, $\vec{\boldsymbol{v}}_s$ and $\vec{\boldsymbol{v}}_{ns}$ are the velocities of the point masses. In the frame $[\vec{\boldsymbol{\imath}},\vec{\boldsymbol{\jmath}}]$ depicted on Fig. A.1, these vectors are given by:

$$\vec{\boldsymbol{v}}_H = -l\dot{\theta}_s\cos\theta_s\vec{\boldsymbol{\imath}}-l\dot{\theta}_s\sin\theta_s\vec{\boldsymbol{\jmath}} \tag{A.4}$$

$$\vec{\boldsymbol{v}}_s = -a\dot{\theta}_s\cos\theta_s\vec{\boldsymbol{\imath}}-a\dot{\theta}_s\sin\theta_s\vec{\boldsymbol{\jmath}} \tag{A.5}$$

$$\vec{\boldsymbol{v}}_{ns} = (b\dot{\theta}_{ns}\cos\theta_{ns}-l\dot{\theta}_s\cos\theta_s)\vec{\boldsymbol{\imath}}+(b\dot{\theta}_{ns}\sin\theta_{ns}-l\dot{\theta}_s\sin\theta_s)\vec{\boldsymbol{\jmath}} \tag{A.6}$$

The first 3 terms appearing in the expression (A.4) for $P(\boldsymbol{\theta})$ have been computed using the horizontal line passing through the tip of the support leg as reference for the gravitational potential energy. This reference line moves after each transition. The scalar P_0, constant during each swing, has been used to keep a constant reference during the compass motion.

Inserting (A.4), (A.5) and (A.6) in (A.2), $K(\boldsymbol{\theta},\dot{\boldsymbol{\theta}})$ can be written as:

$$K(\boldsymbol{\theta},\dot{\boldsymbol{\theta}})=\frac{1}{2}\dot{\boldsymbol{\theta}}^T\boldsymbol{M}(\boldsymbol{\theta})\dot{\boldsymbol{\theta}} \tag{A.7}$$

where $\boldsymbol{M}(\boldsymbol{\theta})$, the inertia matrix of the robot, is given by:

$$\boldsymbol{M}(\boldsymbol{\theta}) = \begin{pmatrix} mb^2 & -mlb\cos(\theta_s - \theta_{ns}) \\ -mlb\cos(\theta_s - \theta_{ns}) & m_H l^2 + m(l^2 + a^2) \end{pmatrix} \tag{A.8}$$

Substituting (A.7), (A.8) and (A.3) in (A.1) leads to the dynamical Equations (2.2) with:

$$\boldsymbol{N}(\boldsymbol{\theta}, \dot{\boldsymbol{\theta}}) = \begin{pmatrix} 0 & mlb\dot{\theta}_s \sin(\theta_s - \theta_{ns}) \\ -mlb\dot{\theta}_{ns} \sin(\theta_s - \theta_{ns}) & 0 \end{pmatrix} \tag{A.9}$$

$$\boldsymbol{g}(\boldsymbol{\theta}) = \begin{pmatrix} mgb \sin\theta_{ns} \\ -(m_H l + m(a+l))g \sin\theta_s \end{pmatrix}. \tag{A.10}$$

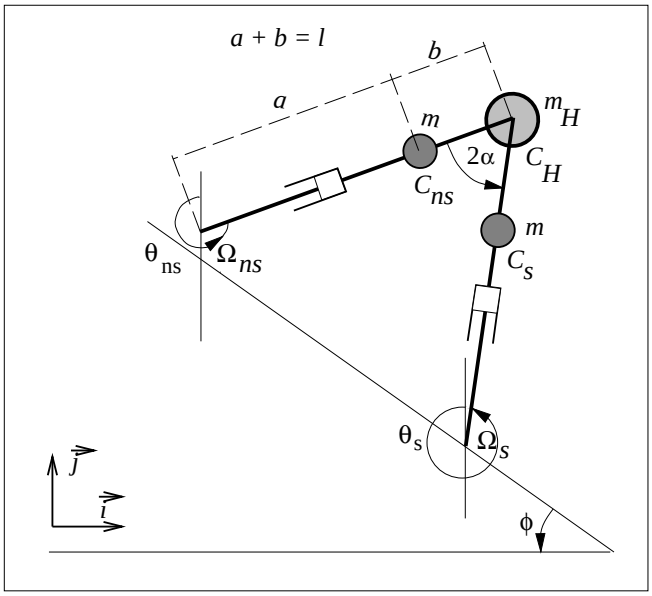

Figure A.1: Additional variables and frames used to describe the compass.

A.2 Linearized swing stage equations

In Section 3.4.2, we are interested in linearizing the Eqs. (2.3) around the system equilibrium $\boldsymbol{q}_e = \mathbf{0}$. The linearized equations are given by:

$$\dot{\boldsymbol{q}} = \begin{pmatrix} \mathbf{0} & \boldsymbol{I}_2 \\ \boldsymbol{A}_b & \end{pmatrix} \boldsymbol{q} \tag{A.11}$$

where the 2×4 matrix $\boldsymbol{A}_b$ is defined by:

$$\boldsymbol{A}_b = - \left(\frac{\partial \boldsymbol{M}^{-1}(\boldsymbol{\theta}) \left[\boldsymbol{N}(\boldsymbol{\theta}, \dot{\boldsymbol{\theta}}) \dot{\boldsymbol{\theta}} + \boldsymbol{g}(\boldsymbol{\theta}) \right]}{\partial \boldsymbol{q}} \right)_{\boldsymbol{q}=\boldsymbol{q}_e} \tag{A.12}$$

Since $\dot{\boldsymbol{\theta}}$ appears in $\boldsymbol{N}(\boldsymbol{\theta}, \dot{\boldsymbol{\theta}})\dot{\boldsymbol{\theta}}$ only as second order terms, $\boldsymbol{A}_b$ is given by:

$$\boldsymbol{A}_b = \left[- \left(\frac{\partial \boldsymbol{M}^{-1}(\boldsymbol{\theta}) \boldsymbol{g}(\boldsymbol{\theta})}{\partial \boldsymbol{\theta}} \right)_{\boldsymbol{q}=\boldsymbol{q}_e} \quad \mathbf{0}_{2\times 2} \right] \tag{A.13}$$

Finally, since $\boldsymbol{M}(\boldsymbol{\theta})$ depends only on $\cos 2\alpha$ and $\boldsymbol{g}(\boldsymbol{\theta})$ depends only on $\sin\theta_{ns}$ or $\sin\theta_s$, we have:

$$\boldsymbol{A}_b = \begin{bmatrix} -\boldsymbol{M}_0^{-1}\boldsymbol{G}_0 & \mathbf{0} \end{bmatrix} \tag{A.14}$$

with:

$$\boldsymbol{M}_0 = \boldsymbol{M}(\boldsymbol{\theta} = \mathbf{0}) = \begin{pmatrix} mb^2 & -mlb \\ -mlb & (m_H l^2 + m(l^2 + a^2)) \end{pmatrix} \tag{A.15}$$

$$\boldsymbol{G}_0 = \begin{pmatrix} mgb & 0 \\ 0 & -(m_H l + m(a+l))g \end{pmatrix} \tag{A.16}$$

Substituting (A.14) in (A.11) leads to expression (3.17) with

$$\boldsymbol{A} = \begin{pmatrix} \mathbf{0} & \boldsymbol{I}_2 \\ -\boldsymbol{M}_0^{-1}\boldsymbol{G}_0 & \mathbf{0} \end{pmatrix} \tag{A.17}$$

A.3 Transition equations

Since our robot is constituted of only two links, the condition of conservation of angular momentum leads to only two equations:

$$m_H\overrightarrow{\Omega_{ns}^- C_H} \wedge \vec{\boldsymbol{v}}_H^- + m(\overrightarrow{\Omega_{ns}^- C_s^-} \wedge \vec{\boldsymbol{v}}_s^- + \overrightarrow{\Omega_{ns}^- C_{ns}^-} \wedge \vec{\boldsymbol{v}}_{ns}^-) \cdots \tag{A.18}$$

$$m_H\overrightarrow{\Omega_s^+ C_H} \wedge \vec{\boldsymbol{v}}_H^+ m(\overrightarrow{\Omega_s^+ C_s^+} \wedge \vec{\boldsymbol{v}}_s^+ + \overrightarrow{\Omega_s^+ C_{ns}^+} \wedge \vec{\boldsymbol{v}}_{ns}^+)$$

$$m\overrightarrow{C_H C_s^-} \wedge \vec{\boldsymbol{v}}_s^- = m\overrightarrow{C_H C_{ns}^+} \wedge \vec{\boldsymbol{v}}_{ns}^+ \tag{A.19}$$

where points C_H, C_{ns}, C_s, Ω_{ns} and Ω_s are respectively the hip, the mass center of the non-support leg, the mass center of the support leg, the tip of the non-support leg and the tip of the support leg (cf. Fig. A.1) and $\vec{\boldsymbol{v}}_H$, $\vec{\boldsymbol{v}}_{ns}$ and $\vec{\boldsymbol{v}}_s$ are respectively the velocity vectors at H, C_{ns} and C_s. The superscripts $^-$ and $^+$ indicate respectively pre-impact and post-impact variables. In the frame $[\vec{\boldsymbol{\imath}}, \vec{\boldsymbol{\jmath}}]$ depicted in Fig. A.1, all the vectors appearing in (A.18) and (A.19) are given by:

$$\overrightarrow{\Omega_{ns}^- C_H} = -l\sin\theta_{ns}^-\vec{\boldsymbol{\imath}} + l\cos\theta_{ns}^-\vec{\boldsymbol{\jmath}} \tag{A.20}$$

$$\overrightarrow{\Omega_s^+ C_H} = -l\sin\theta_s^+\vec{\boldsymbol{\imath}} + l\cos\theta_s^+\vec{\boldsymbol{\jmath}} \tag{A.21}$$

$$\overrightarrow{\Omega_{ns}^- C_s^-} = (b\sin\theta_s^- - l\sin\theta_{ns}^-)\vec{\boldsymbol{\imath}} + (l\cos\theta_{ns}^- - b\cos\theta_s^-)\vec{\boldsymbol{\jmath}} \tag{A.22}$$

$$\overrightarrow{\Omega_s^+ C_{ns}^+} = (b\sin\theta_{ns}^+ - l\sin\theta_s^+)\vec{\boldsymbol{\imath}} + (l\cos\theta_s^+ - b\cos\theta_{ns}^+)\vec{\boldsymbol{\jmath}} \tag{A.23}$$

$$\overrightarrow{\Omega_{ns}^- C_{ns}^-} = -a\sin\theta_{ns}^-\vec{\boldsymbol{\imath}} + a\cos\theta_{ns}^-\vec{\boldsymbol{\jmath}} \tag{A.24}$$

$$\overrightarrow{\Omega_s^+ C_s^+} = -a\sin\theta_s^+\vec{\boldsymbol{\imath}} + a\cos\theta_s^+\vec{\boldsymbol{\jmath}} \tag{A.25}$$

$$\overrightarrow{C_H C_s^-} = b\sin\theta_s^-\vec{\boldsymbol{\imath}} - b\cos\theta_s^-\vec{\boldsymbol{\jmath}} \tag{A.26}$$

$$\overrightarrow{C_H C_{ns}^+} = b\sin\theta_{ns}^+\vec{\boldsymbol{\imath}} - b\cos\theta_{ns}^+\vec{\boldsymbol{\jmath}} \tag{A.27}$$

$$\vec{\boldsymbol{v}}_h^- = -l\dot{\theta}_s^-\cos\theta_s^-\vec{\boldsymbol{\imath}} - l\dot{\theta}_s^-\sin\theta_s^-\vec{\boldsymbol{\jmath}} \tag{A.28}$$

$$\vec{\boldsymbol{v}}_h^+ = -l\dot{\theta}_s^+\cos\theta_s^+\vec{\boldsymbol{\imath}} - l\dot{\theta}_s^+\sin\theta_s^+\vec{\boldsymbol{\jmath}} \tag{A.29}$$

$$\vec{\boldsymbol{v}}_s^- = -a\dot{\theta}_s^-\cos\theta_s^-\vec{\boldsymbol{\imath}} - a\dot{\theta}_s^-\sin\theta_s^-\vec{\boldsymbol{\jmath}} \tag{A.30}$$

$$\vec{\boldsymbol{v}}_s^+ = -a\dot{\theta}_s^+\cos\theta_s^+\vec{\boldsymbol{\imath}} - a\dot{\theta}_s^+\sin\theta_s^+\vec{\boldsymbol{\jmath}} \tag{A.31}$$

$$\vec{\boldsymbol{v}}_{ns}^- = (b\dot{\theta}_{ns}^-\cos\theta_{ns}^- - l\dot{\theta}_s^-\cos\theta_s^-)\vec{\boldsymbol{\imath}} + (b\dot{\theta}_{ns}^-\sin\theta_{ns}^- - l\dot{\theta}_s^-\sin\theta_s^-)\vec{\boldsymbol{\jmath}} \tag{A.32}$$

$$\vec{\boldsymbol{v}}_{ns}^+ = (b\dot{\theta}_{ns}^+\cos\theta_{ns}^+ - l\dot{\theta}_s^+\cos\theta_s^+)\vec{\boldsymbol{\imath}} + (b\dot{\theta}_{ns}^+\sin\theta_{ns}^+ - l\dot{\theta}_s^+\sin\theta_s^+)\vec{\boldsymbol{\jmath}} \tag{A.33}$$

Substituting the Eqs. (A.20) to (A.33) and the Eq. (2.10) in (A.18) and (A.19), we get the following compact Equation between the pre-impact and post-impact angular velocities:

$$\boldsymbol{Q}^-(\alpha)\dot{\boldsymbol{\theta}}^- = \boldsymbol{Q}^+(\alpha)\dot{\boldsymbol{\theta}}^+ \tag{A.34}$$

with matrices $\boldsymbol{Q}^-(\alpha)$ and $\boldsymbol{Q}^+(\alpha)$ given by:

$$\boldsymbol{Q}^-(\alpha) = \begin{pmatrix} -mab & -mab + (m_H l^2 + 2mal)\cos 2\alpha \\ 0 & -mab \end{pmatrix} \quad \text{(A.35)}$$

$$\boldsymbol{Q}^+(\alpha) = \begin{pmatrix} mb(b - l\cos 2\alpha) & ml(l - b\cos 2\alpha) + ma^2 + m_H l^2 \\ mb^2 & -mbl\cos 2\alpha \end{pmatrix} \quad \text{(A.36)}$$

Let us finally introduce matrix $\boldsymbol{H}(\alpha)$ as:

$$\boldsymbol{H}(\alpha) = \boldsymbol{Q}^{+\,-1}(\alpha)\boldsymbol{Q}^-(\alpha) \quad \text{(A.37)}$$

A.4 Normalization of the compass equations

In this report, we make essentially make use of normalized equations of the compass biped. The proofs of Property 2.1, normalization process, and Properties 2.2 and 2.3, normalization consequences, are provided below:

Proof of Property 2.1:

Normalized equations of the compass biped consist of Eqs. (2.2), (A.35) and (A.36) from which ma^2 has been factored out.

Normalized swing equations:

Eqs. (2.2) can also be written as:

$$ma^2\left[\boldsymbol{M}_n(\boldsymbol{\theta})\ddot{\boldsymbol{\theta}} + \boldsymbol{N}_n(\boldsymbol{\theta},\dot{\boldsymbol{\theta}})\dot{\boldsymbol{\theta}} + \frac{1}{a}\boldsymbol{g}_n(\boldsymbol{\theta})\right] = \mathbf{0} \quad \text{(A.38)}$$

where:

$$\boldsymbol{M}_n(\boldsymbol{\theta}) = \begin{pmatrix} \beta^2 & -(1+\beta)\,\beta\cos 2\alpha \\ -(1+\beta)\,\beta\cos 2\alpha & \mu\,(1+\beta)^2 + \left(1 + (1+\beta)^2\right) \end{pmatrix} \quad \text{(A.39)}$$

$$\boldsymbol{N}_n(\boldsymbol{\theta},\dot{\boldsymbol{\theta}}) = \begin{pmatrix} 0 & (1+\beta)\,\beta\dot{\theta}_s \sin(\theta_s - \theta_{ns}) \\ -(1+\beta)\,\beta\dot{\theta}_{ns}\sin(\theta_s - \theta_{ns}) & 0 \end{pmatrix} \quad \text{(A.40)}$$

$$\boldsymbol{g}_n(\boldsymbol{\theta}) = \begin{pmatrix} g\beta\sin\theta_{ns} \\ -(\mu\,(1+\beta) + (1 + (1+\beta)))\,g\sin\theta_s \end{pmatrix} \quad \text{(A.41)}$$

$\boldsymbol{M}_n(\boldsymbol{\theta})$, $\boldsymbol{N}_n(\boldsymbol{\theta},\dot{\boldsymbol{\theta}})$ and $\boldsymbol{g}_n(\boldsymbol{\theta})$ do not depend on m, m_H, b or a, but only on μ and β.

Normalized transition equations:

Eqs. (A.35) and (A.36) can also be written as:

$$\boldsymbol{Q}_n^-(\alpha) = ma^2 \begin{pmatrix} -\beta & -\beta + \left(\mu\,(1+\beta)^2 + 2\,(1+\beta)\right)\cos 2\alpha \\ 0 & -\beta \end{pmatrix} \quad \text{(A.42)}$$

$$\boldsymbol{Q}_n^+(\alpha) = ma^2 \begin{pmatrix} \beta\,(\beta - (1+\beta)\cos 2\alpha) & (1+\beta)\,((1+\beta) - \beta\cos 2\alpha) \\ & \cdots + 1 + \mu\,(1+\beta)^2 \\ \beta^2 & -\beta\,(1+\beta)\cos 2\alpha \end{pmatrix} \quad \text{(A.43)}$$

which renders the transition equations normalized. ◇

Proof of Property 2.2:

Let us name $\mathcal{C}_m^{'}$ and $\mathcal{C}_m$ robots with masses respectively $\left(m^{'}, m_H\frac{m^{'}}{m}\right)$ and (m, m_H), and $\boldsymbol{\theta}_m^{'}(t),\ t \in [0, T^{'}]$ and $\boldsymbol{\theta}_m(t),\ t \in [0, T]$, their respective time-evolution during one swing, starting from identical initial conditions: $\boldsymbol{\theta}_m(0) = \boldsymbol{\theta}_m^{'}(0)$.

The scalars μ associated with robots $\mathcal{C}_m^{'}$ and $\mathcal{C}_m$ are obviously equal. Therefore, since $\boldsymbol{M}_n(\boldsymbol{\theta})$, $\boldsymbol{N}_n(\boldsymbol{\theta}, \dot{\boldsymbol{\theta}})$ and $\boldsymbol{g}_n(\boldsymbol{\theta})$ depend only on μ, we deduce immediately from (2.11) that $T = T^{'}$ and $\boldsymbol{\theta}_m(t) = \boldsymbol{\theta}_m^{'}(t)$, $\forall t \in [0, T^{'}]$. Moreover, since matrix $\boldsymbol{W}(\alpha)$ depends also only on μ, the post-impact state vectors $\boldsymbol{\theta}_m(T^{+'})$ and $\boldsymbol{\theta}_m^{'}(T^{+'})$, which are also the initial conditions for the following swing, are equal as well. This discussion proves clearly that the time-evolutions of the robots $\mathcal{C}_m^{'}$ and $\mathcal{C}_m$ remain identical when their initial conditions are equal. Therefore, as stated in Property 2.2, passive gait analysis can be achieved by varying only the mass ratio μ. The table in Property 2.2 follows from $\boldsymbol{\theta}_m(t) = \boldsymbol{\theta}_m^{'}(t)$, $\forall t$, Eqs. (2.10), (A.2) and (A.3) and definition of L and v (page 15). ◇

Proof of Property 2.3:

Let us name $\mathcal{C}_a^{'}$ and $\mathcal{C}_a$ robots with lengths respectively $\left(a^{'}, b\frac{a^{'}}{a}\right)$ and (a, b), and $\boldsymbol{\theta}_a^{'}(t),\ t \in [0, T^{'}]$ and $\boldsymbol{\theta}_a(t),\ t \in [0, T]$, their respective time-evolution during one swing, when both initial conditions are equal: $\boldsymbol{\theta}_a(0) = \boldsymbol{\theta}_a^{'}(0)$.

The time functions $\boldsymbol{\theta}_a^{'}(t)$ and $\boldsymbol{\theta}_a(t)$ are the solutions of the dynamic equations:

$$\boldsymbol{\theta}_a^{'}(t) \ : \ \boldsymbol{M}_n(\boldsymbol{\theta}) \begin{pmatrix} \ddot{\theta}_{ns} \\ \ddot{\theta}_s \end{pmatrix} + \boldsymbol{N}_n(\boldsymbol{\theta}, \dot{\theta}_{ns}, \dot{\theta}_s) \begin{pmatrix} \dot{\theta}_{ns} \\ \dot{\theta}_s \end{pmatrix} + \frac{1}{a^{'}}\,\boldsymbol{g}_n(\boldsymbol{\theta}) = 0 \quad \text{(A.44)}$$

$$\boldsymbol{\theta}_a(t) \ : \ \boldsymbol{M}_n(\boldsymbol{\theta}) \begin{pmatrix} \ddot{\theta}_{ns} \\ \ddot{\theta}_s \end{pmatrix} + \boldsymbol{N}_n(\boldsymbol{\theta}, \dot{\theta}_{ns}, \dot{\theta}_s) \begin{pmatrix} \dot{\theta}_{ns} \\ \dot{\theta}_s \end{pmatrix} + \frac{1}{a}\,\boldsymbol{g}_n(\boldsymbol{\theta}) = 0 \quad \text{(A.45)}$$

In order to point out the connection between $\boldsymbol{\theta}_a^{'}(t)$ and $\boldsymbol{\theta}_a(t)$, let us introduce the following time scale factor:

$$t' = \sqrt{k_a}t \tag{A.46}$$

Using (A.46), Eq. (A.44) can also be written as:

$$\begin{aligned}\boldsymbol{\theta}_a^{'}(t) \quad : \quad & \boldsymbol{M}_n(\boldsymbol{\theta})\left(\frac{d\,t'}{d\,t}\right)^2 \begin{pmatrix} \frac{d^2\,\theta_{ns}}{d\,t'^2} \\ \frac{d^2\,\theta_s}{d\,t'^2} \end{pmatrix} + \boldsymbol{N}_n\left(\boldsymbol{\theta}, \frac{d\,t'}{d\,t}\frac{d\,\theta_{ns}}{d\,t'}, \frac{d\,t'}{d\,t}\frac{d\,\theta_s}{d\,t'}\right)\frac{d\,t'}{d\,t}\begin{pmatrix} \frac{d\,\theta_{ns}}{d\,t'} \\ \frac{d\,\theta_s}{d\,t'} \end{pmatrix} \\ & + \frac{1}{a'}\,\boldsymbol{g}_n(\boldsymbol{\theta}) = 0\end{aligned} \tag{A.47}$$

In view of (A.40), we have:

$$\boldsymbol{N}\left(\boldsymbol{\theta}, \frac{d\,t'}{d\,t}\frac{d\,\theta_{ns}}{d\,t'}, \frac{d\,t'}{d\,t}\frac{d\,\theta_s}{d\,t'}\right) = \frac{d\,t'}{d\,t}\boldsymbol{N}\left(\boldsymbol{\theta}, \frac{d\,\theta_{ns}}{d\,t'}, \frac{d\,\theta_s}{d\,t'}\right) \tag{A.48}$$

Using (A.48) and Eqs. (2.12) and (A.46), Eq. (A.47) can be simplified as:

$$\boldsymbol{\theta}_a^{'} \; : \; k_a\left[\boldsymbol{M}_n(\boldsymbol{\theta})\begin{pmatrix} \frac{d^2\,\theta_{ns}}{d\,t'^2} \\ \frac{d^2\,\theta_s}{d\,t'^2} \end{pmatrix} + \boldsymbol{N}_n\left(\boldsymbol{\theta}, \frac{d\,\theta_{ns}}{d\,t'}, \frac{d\,\theta_s}{d\,t'}\right)\begin{pmatrix} \frac{d\,\theta_{ns}}{d\,t'} \\ \frac{d\,\theta_s}{d\,t'} \end{pmatrix} + \frac{1}{a}\,\boldsymbol{g}_n(\boldsymbol{\theta})\right] = 0 \tag{A.49}$$

Comparing now Eqs. (A.49) and (A.45) and using (A.46), we conclude that:

$$T = \sqrt{k_a}T^{'} \qquad \boldsymbol{\theta}_a(t) = \boldsymbol{\theta}_a^{'}\left(\frac{t}{\sqrt{k_a}}\right) \quad t \in [0, \sqrt{k_a}T^{'}] \tag{A.50}$$

Therefore, as stated in Property 2.3, passive gait analysis can be achieved by varying only the length ratio β. The table in Property 2.3 follows from (A.50), Eqs. (2.10), (A.2) and (A.3) and definition of L and v (page 15). $\diamond$

B Loss of energy during the transition (proof)

Since the Assumptions A6-A7 (page 14) does not explicitly provide any information on the energy balance of the transition, we prove below that the mechanical energy E is, as expected, strictly decreasing or, in few special situations, conserved. These computations show that our description of the leg impact on the ground, which leads to quite simple equations, is nevertheless realistic.

Since, on one hand, the robot potential energy P is a function of θ_{ns} and θ_s only (cf. Eq. (A.3)), and, on the other hand, these two quantities are kept unchanged

during the double-support stage (Eq. (2.4)), P is conserved through this stage. Therefore, the variation of the robot mechanical energy E consists only of the variation of the kinetic energy K. Using (A.7), we have then:

$$\Delta E(\boldsymbol{\theta}, \dot{\boldsymbol{\theta}}) = \dot{\boldsymbol{\theta}}^{+\,T} \boldsymbol{M}(\boldsymbol{\theta}^+) \dot{\boldsymbol{\theta}}^+ - \dot{\boldsymbol{\theta}}^{-\,T} \boldsymbol{M}(\boldsymbol{\theta}^-) \dot{\boldsymbol{\theta}}^- \tag{B.1}$$

By reporting (2.6) in (B.1), this Equation can also be written as:

$$\Delta E(\boldsymbol{\theta}, \dot{\boldsymbol{\theta}}) = \dot{\boldsymbol{\theta}}^{-\,T} (\boldsymbol{H}^T(\alpha) \boldsymbol{M}(\boldsymbol{\theta}^+) \boldsymbol{H}(\alpha) - \boldsymbol{M}(\boldsymbol{\theta}^-)) \dot{\boldsymbol{\theta}}^- \tag{B.2}$$

By reporting now (2.10) in (A.8), we see clearly that:

$$\boldsymbol{M}(\boldsymbol{\theta}^-) = \boldsymbol{M}(\boldsymbol{\theta}^+) = \boldsymbol{M}(\alpha) \tag{B.3}$$

Finally, reporting (B.3) in (B.2) leads to:

$$\Delta E(\alpha, \dot{\boldsymbol{\theta}}) = \dot{\boldsymbol{\theta}}^{-\,T} (\boldsymbol{H}^T(\alpha) \boldsymbol{M}(\alpha) \boldsymbol{H}(\alpha) - \boldsymbol{M}(\alpha)) \dot{\boldsymbol{\theta}}^- \tag{B.4}$$

Using (A.8), (A.35), (A.36), (A.37) and running *Maple V* software [Map94], it can be proved that the explicit expression for (B.4), when $\dot{\theta}_s \neq 0$, is:

$$\Delta E(\alpha, \dot{\boldsymbol{\theta}}) = \frac{m a^2 \dot{\theta}_s^{-2} \Lambda(\alpha, \eta, \mu, \beta)}{\beta^2(1 - \cos^2 2\alpha) + 2\beta(1 - \cos^2 2\alpha) + (1 - \cos^2 2\alpha) + 1 + \mu\beta^2 + 2\mu\beta + \mu} \tag{B.5}$$

with:

$$\begin{aligned}
\Lambda(\alpha, \eta, \mu, \beta) \;=\; & -2 + 6\beta\cos^2 2\alpha + 7\beta^2\cos^2 2\alpha + 12\mu\beta^2\cos^2 2\alpha + 10\mu\beta\cos^2 2\alpha \\
& + \beta^4\mu\cos^2 2\alpha - 3\mu + 3\mu\cos^2 2\alpha + \mu^2\cos^2 2\alpha - 2\beta^4\mu - \beta^4 \\
& - 4\beta^3\mu^2 - 8\beta^3\mu - 4\beta^3 - 6\beta - \beta^4\eta^2 - \beta^4\mu^2 - 7\beta^2 + 4\beta^3\cos^2 2\alpha \\
& + \beta^4\cos^2 2\alpha + 6\beta^3\mu\cos^2 2\alpha + \beta^4\mu^2\cos^2 2\alpha + 4\beta^3\mu^2\cos^2 2\alpha \\
& - 6\beta^3\eta\cos^3 2\alpha - 2\beta^4\eta\cos^3 2\alpha + 6\beta^3\eta\cos 2\alpha + 2\eta^2\beta^3\cos^2 2\alpha \\
& + \beta^4\eta^2\cos^2 2\alpha + 2\beta^4\eta\cos 2\alpha + 2\beta^4\eta\mu\cos 2\alpha + 4\eta\beta^3\mu\cos 2\alpha \\
& - 13\mu\beta^2 - 10\mu\beta + 2\cos^2 2\alpha - 4\mu^2\beta - 6\mu^2\beta^2 - 2\eta^2\beta^3 - \mu^2 \\
& - \eta^2\beta^2 - \eta^2\beta^2\mu + 2\eta\beta^2\mu\cos 2\alpha + 6\mu^2\beta^2\cos^2 2\alpha + 4\mu^2\beta\cos^2 2\alpha \\
& - 2\eta\beta\cos^3 2\alpha - 6\eta\beta^2\cos^3 2\alpha + 2\eta\beta\cos 2\alpha + 6\eta\beta^2\cos 2\alpha \\
& - 2\eta^2\beta^3\mu - \beta^4\eta^2\mu + \eta^2\beta^2\cos^2 2\alpha
\end{aligned} \tag{B.6}$$

The scalars β and μ have been defined before and η is given by:

$$\eta = \frac{\dot{\theta}_{ns}^-}{\dot{\theta}_s^-} \qquad \text{when } \dot{\theta}_s^- \neq 0 \tag{B.7}$$

When $\dot{\theta}_s^- = 0$, the explicit expression for ΔE is by far more simple. Symbolic computations, running *Maple V* software, lead to:

$$\Delta E(\alpha, \dot{\boldsymbol{\theta}}) = -mb^2 l^2 \dot{\theta}_{ns}^{-2} \frac{m(1-\cos^2 2\alpha) + m_H}{ml^2(1-\cos^2 2\alpha) + ma^2 + m_H l^2} \tag{B.8}$$

When $\dot{\theta}_s^- = 0$, the variation of the robot mechanical energy E during the transition, in view of (B.8), is clearly non-increasing. More precisely, E is strictly decreasing, except in the special situation $\dot{\boldsymbol{\theta}}^- = 0$.

We now prove a similar result in the case $\dot{\theta}_s^- \neq 0$. The denominator of ΔE in (B.5), since β and μ are positive, is obviously strictly positive. $ma^2\dot{\theta}_s^{-2}$, since we assume here that $\dot{\theta}_s^{-2} \neq 0$, is also strictly positive. The sign of $\Delta E(\alpha, \dot{\boldsymbol{\theta}})$ depends therefore only on the sign of $\Lambda(\alpha, \eta, \mu, \beta)$. This function can be written as a parabola in the variable μ:

$$\Lambda(\alpha, \eta, \mu, \beta) = \kappa_2(\alpha, \eta, \beta)\mu^2 + \kappa_1(\alpha, \eta, \beta)\mu + \kappa_0(\alpha, \eta, \beta) \tag{B.9}$$

We show below that the functions $\kappa_i(\alpha, \eta, \beta)_{i\in\{1,2,3\}}$ are all negative, which prove, since μ is positive, that $\Delta E(\alpha, \dot{\boldsymbol{\theta}})$ is non increasing as expected.

Let us consider first $\kappa_2(\alpha, \eta, \beta)$. Using (B.6), we obtain that:

$$\kappa_2(\alpha, \eta, \beta) = -(1-\cos^2 2\alpha)(1 - 4\beta - 6\beta^2 - 4\beta^3 - \beta^4) \tag{B.10}$$

Since β is positive, Eq. (B.10) shows clearly that the values of $\kappa_2(\alpha, \eta, \beta)$ are always strictly negative, except in the special situation $\alpha = 0\ [\frac{\pi}{2}]$, where $\kappa_2(\alpha, \eta, \beta)$ is then zero.

Let us consider now $\kappa_1(\alpha, \eta, \beta)$. Using (B.6), we obtain that:

$$\kappa_1(\alpha, \eta, \beta) = \sigma_0(\eta, \alpha) + \sigma_1(\eta, \alpha)\,\beta + \sigma_2(\eta, \alpha)\,\beta^2 + \sigma_3(\eta, \alpha)\,\beta^3 + \sigma_4(\eta, \alpha)\,\beta^4 \tag{B.11}$$

with:

$$\sigma_0(\eta,\alpha) = -3(1-\cos^2 2\alpha) \quad \text{(B.12)}$$
$$\sigma_1(\eta,\alpha) = -10(1-\cos^2 2\alpha) \quad \text{(B.13)}$$
$$\sigma_2(\eta,\alpha) = -13+12\cos^2 2\alpha+2\eta\cos 2\alpha-\eta^2 \quad \text{(B.14)}$$
$$\sigma_3(\eta,\alpha) = -8+6\cos^2 2\alpha+4\eta\cos 2\alpha-2\eta^2 \quad \text{(B.15)}$$
$$\sigma_4(\eta,\alpha) = -2+\cos^2 2\alpha+2\eta\cos 2\alpha-\eta^2 \quad \text{(B.16)}$$

The values of $\sigma_0(\eta,\alpha)$ and $\sigma_1(\eta,\alpha)$, Eqs. (B.12) and (B.13), are obviously always strictly negative, except in the special situation $\alpha = 0\ [\frac{\pi}{2}]$, where these functions are then zero.

The remaining functions $\sigma_i(\eta,\alpha)_{i\in\{2,3,4\}}$ (Eqs. (B.14), (B.15) and (B.16)) can be seen as parabolas in the variable η. Their extremum occurs for $\eta = \cos 2\alpha$ (just compute η / $\frac{\partial \sigma_i(\eta,\alpha)_{i\in\{2,3,4\}}}{\partial \eta} = 0$). More precisely, it is always a maximum since $\frac{\partial^2 \sigma_i(\eta,\alpha)_{i\in\{2,3,4\}}}{\partial \eta^2}$ is constant for all η and strictly negative. Finally, since $\sigma_2(\eta,\alpha)$, $\sigma_3(\eta,\alpha)$ and $\sigma_4(\eta,\alpha)$ at $\eta = \cos 2\alpha$ are equal respectively to $-13(1-\cos^2 2\alpha)$, $-8(1-\cos^2 2\alpha)$ and $-2(1-\cos^2 2\alpha)$, we conclude that the values of $\sigma_i(\eta,\alpha)_{i\in\{2,3,4\}}$ are always strictly negative, except in the special situation $\alpha = 0\ [\frac{\pi}{2}]$, where these functions are zero if $\eta = \cos 2\alpha$.

Since β is positive, it is then obvious, in view of (B.11), that the values of $\kappa_1(\alpha,\eta,\beta)$ are strictly negative, except in the special situation $\alpha = 0\ [\frac{\pi}{2}]$, where $\kappa_1(\alpha,\eta,\beta)$ is zero if $\eta = \cos 2\alpha$ or $\beta = 0$.

Let us finally consider $\kappa_0(\alpha,\eta,\beta)$. Using (B.6), we obtain that:

$$\kappa_0(\alpha,\eta,\beta) = \sigma_5(\beta,\alpha)\,\eta^2 + \sigma_6(\beta,\alpha)\,\eta + \sigma_7(\beta,\alpha) \quad \text{(B.17)}$$

with:

$$\sigma_5(\beta,\alpha) = -(1-\cos^2 2\alpha)(\beta^4+2\beta^3+\beta^2) \quad \text{(B.18)}$$
$$\sigma_6(\beta,\alpha) = \cos 2\alpha(1-\cos^2 2\alpha)(2\beta^4+6\beta^3+6\beta^2+2\beta) \quad \text{(B.19)}$$
$$\sigma_7(\beta,\alpha) = -(1-\cos^2 2\alpha)(\beta^4+4\beta^3+7\beta^2+6\beta+2) \quad \text{(B.20)}$$

In the case $\alpha = 0\ [\frac{\pi}{2}]$, $\kappa_0(\alpha,\eta,\beta)$ (Eqs. (B.17), (B.18), (B.19) and (B.20)) is obviously zero. In the case $\beta = 0$, $\kappa_0(\alpha,\eta,\beta)$ (Eqs. (B.17), (B.18), (B.19) and (B.20)) is a constant strictly negative, except of course if $\alpha = 0\ [\frac{\pi}{2}]$, since $\kappa_0(\alpha,\eta,\beta)$ is then zero. Otherwise, this function is a parabola in the variable η (Eq. (B.17)), whose

extremum occurs for (just derive Eq. (B.17)):

$$\eta = \frac{\sigma_6(\beta,\alpha)}{2\sigma_5(\beta,\alpha)} \tag{B.21}$$

More precisely, this extremum is a maximum since:

$$\frac{\partial^2 \kappa_0(\alpha,\eta,\beta)}{\partial \eta^2} = 2\sigma_5(\beta,\alpha) \tag{B.22}$$

and $\sigma_5(\beta,\alpha)$ is strictly negative (β is positive and we assume here that $\beta \neq 0$). Reporting (B.21) in (B.17) provides us with the maximum value for $\kappa_0(\alpha,\eta,\beta)$:

$$\begin{aligned} \kappa_0^{max}(\beta,\alpha) &= -(1-\cos^2 2\alpha)\left(-\frac{(\beta^4+3\beta^3+3\beta^2+\beta)^2}{\beta^4+2\beta^3+\beta^2}\cos^2 2\alpha + \cdots\right. \\ &\quad \left.\cdots \beta^4+4\beta^3+7\beta^2+6\beta+2\right) \end{aligned} \tag{B.23}$$

It can be easily verified that:

$$\left(-\frac{(\beta^4+3\beta^3+3\beta^2+\beta)^2}{\beta^4+2\beta^3+\beta^2}+\beta^4+4\beta^3+7\beta^2+6\beta+2\right) = (\beta+1)^2 \tag{B.24}$$

We conclude from (B.23) and (B.24) that the values of $\kappa_0(\alpha,\eta,\beta)$ are always strictly negative when $\alpha \neq 0 \ [\frac{\pi}{2}]$. In this latter special situation, as mentioned before, $\kappa_0(\alpha,\eta,\beta)$ is then zero.

The sign of functions $\kappa_i(\alpha,\eta,\beta)_{i\in\{0,1,2\}}$ has now been investigated. Since μ is positive, the results obtained above ensure (just consider Eqs. (B.5), (B.9) and (B.8)) that during the transition:

- The total mechanical energy E is conserved in the special situations:
  - $\dot{\boldsymbol{\theta}} = 0$
  - $\begin{cases} \alpha = 0 \ [\frac{\pi}{2}] \\ \mu = 0 \end{cases}$
  - $\begin{cases} \alpha = 0 \ [\frac{\pi}{2}] \\ \beta = 0 \end{cases}$
  - $\begin{cases} \alpha = 0 \ [\frac{\pi}{2}] \\ \eta = \cos 2\alpha = 1 \end{cases}$
- E is strictly decreasing otherwise.

C Graphs

C.1 Comparison between the non-linear and the linearized compass models

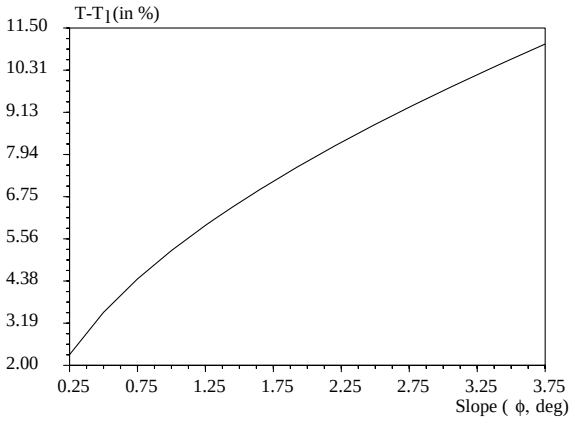

Figure C.1: *Comparison between the nonlinear and the linearized compass models:* difference in the step period T as a function of ground slope ϕ.

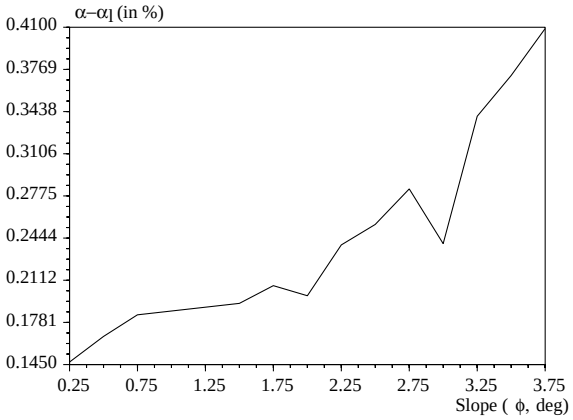

Figure C.2: *Comparison between the nonlinear and the linearized compass models:* difference in the half inter-leg angle α as a function of ground slope ϕ.

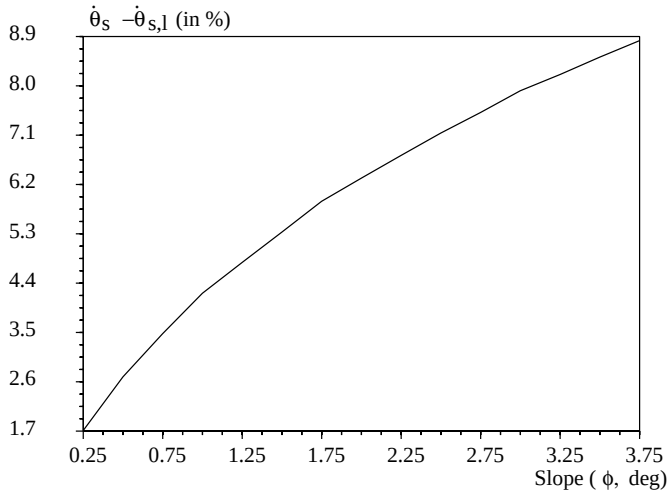

Figure C.3: *Comparison between the nonlinear and the linearized compass models:* difference in the support leg angle velocity $\dot{\theta}_s$ as a function of ground slope ϕ.

C.2 Bifurcation and phase plane diagrams related to the parameter ϕ

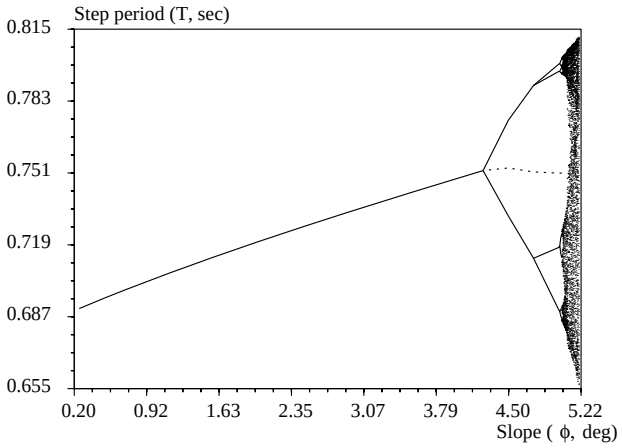

Figure C.4: *Bifurcation diagram* : step period T as a function of ground slope ϕ ($\mu = 2, \beta = 1$).

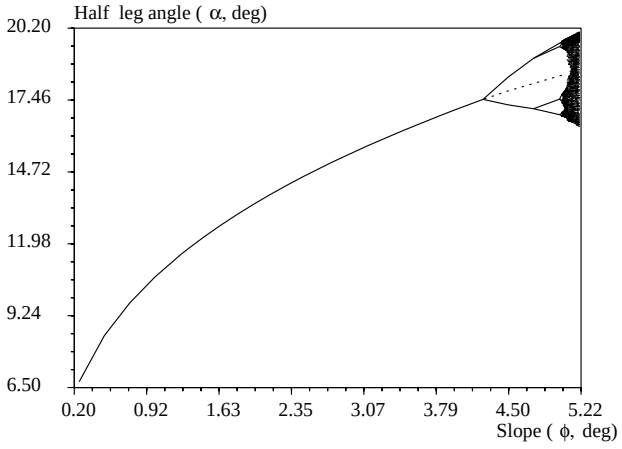

Figure C.5: *Bifurcation diagram* : half inter-leg angle α as a function of ground slope ϕ ($\mu = 2, \beta = 1$).

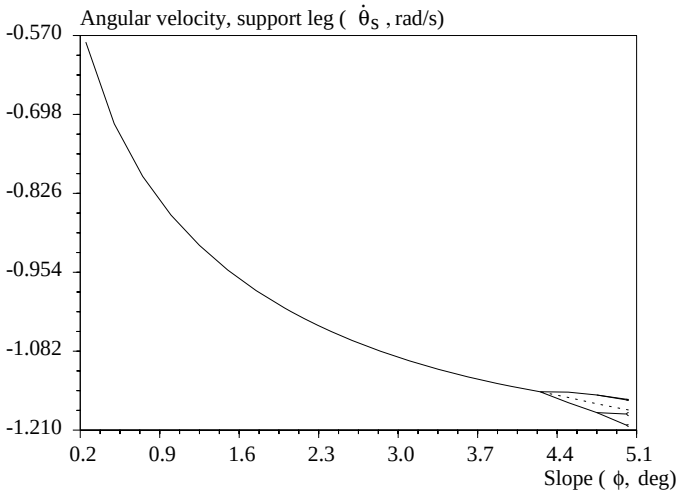

Figure C.6: *Bifurcation diagram* : angular velocity of the support leg $\dot{\theta}_s$ as a function of ground slope ϕ ($\mu = 2, \beta = 1$).

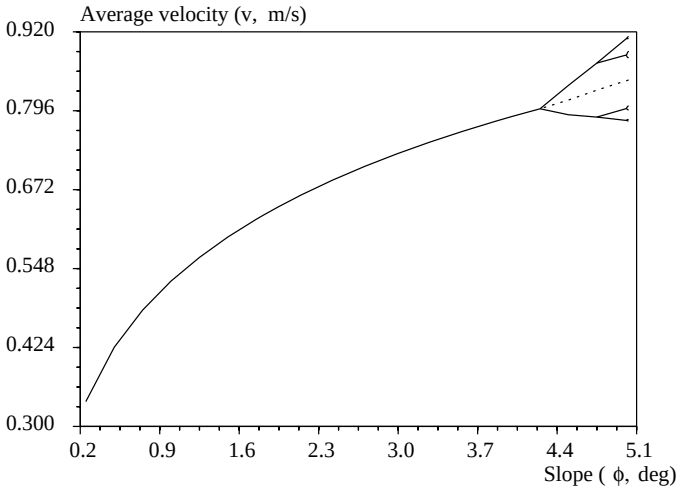

Figure C.7: *Bifurcation diagram* : average speed of progression v as a function of ground slope ϕ ($\mu = 2, \beta = 1$).

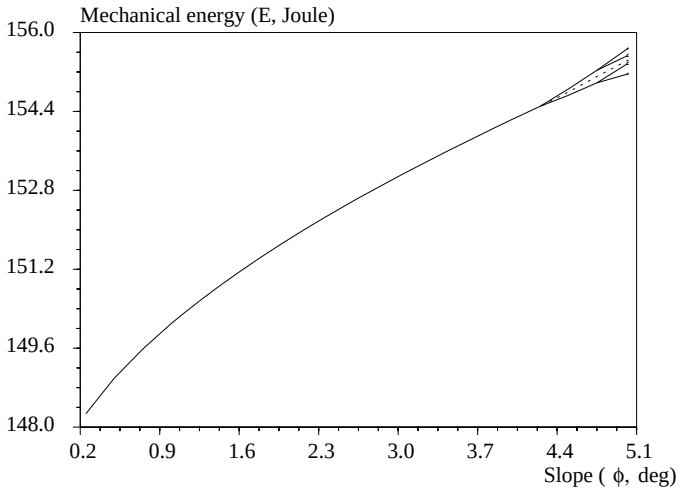

Figure C.8: *Bifurcation diagram* : mechanical energy E as a function of ground slope ϕ ($\mu = 2, \beta = 1$).

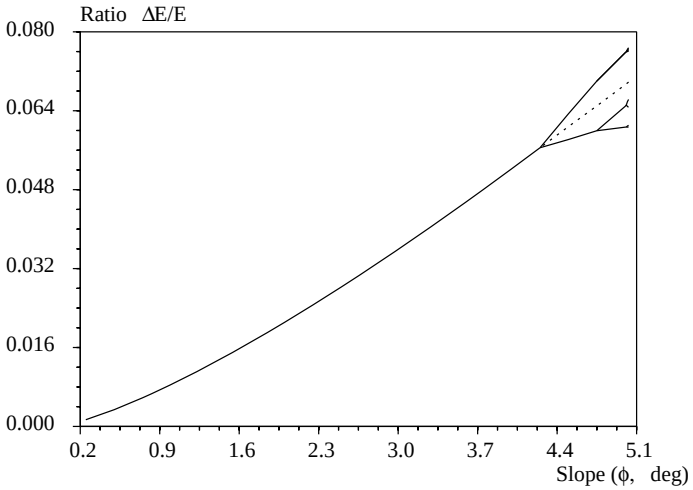

Figure C.9: *Bifurcation diagram* : ratio $\frac{\Delta E}{E}$ as a function of ground slope ϕ ($\mu = 2, \beta = 1$).

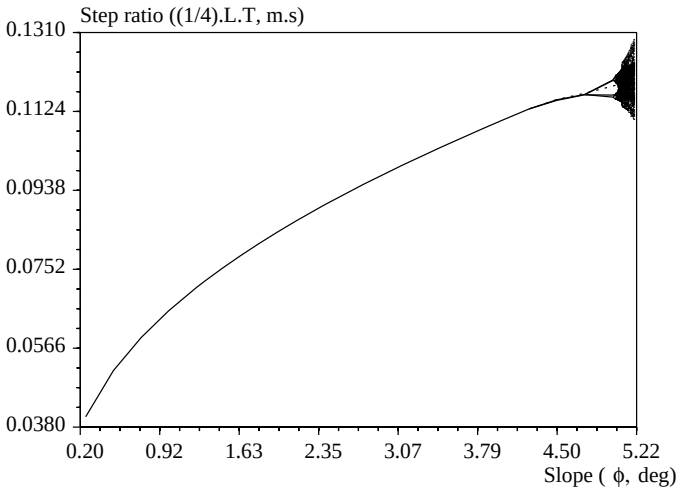

Figure C.10: *Bifurcation diagram* : step ratio $\frac{LT}{4}$ as a function of ground slope ϕ $(\mu = 2, \beta = 1)$.

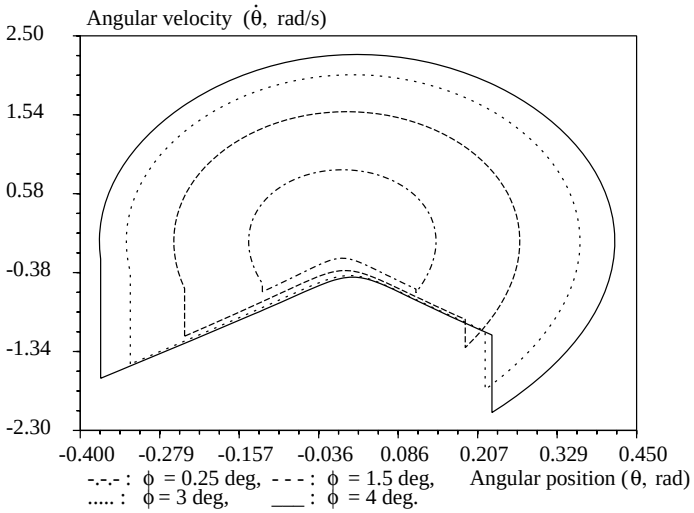

Figure C.11: *Phase plane limit cycles* for $\phi = 0.25^o$, 1.5^o, 3^o and 4^o $(\mu = 2, \beta = 1)$.

C.3 Bifurcation and phase plane diagrams related to the parameter μ

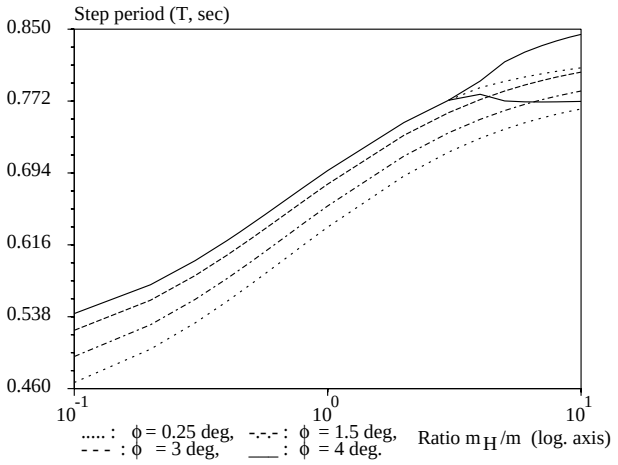

Figure C.12: *Bifurcation diagram* : step period T as a function of μ ($\beta = 1, \phi = 0.25^o, 1.5^o, 3^o$ and 4^o).

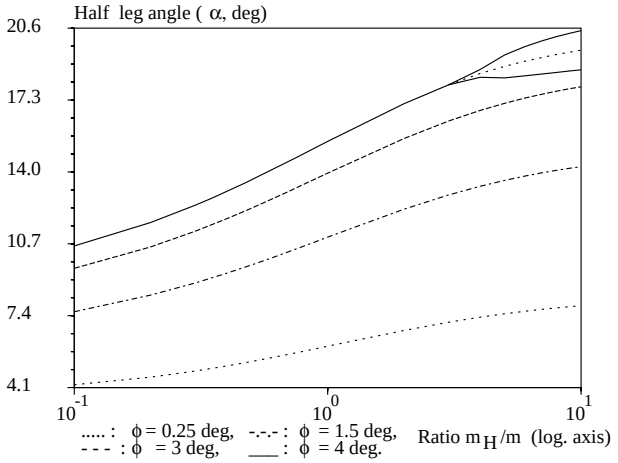

Figure C.13: *Bifurcation diagram* : half inter-leg angle α as a function of μ ($\beta = 1, \phi = 0.25^o, 1.5^o, 3^o$ and 4^o).

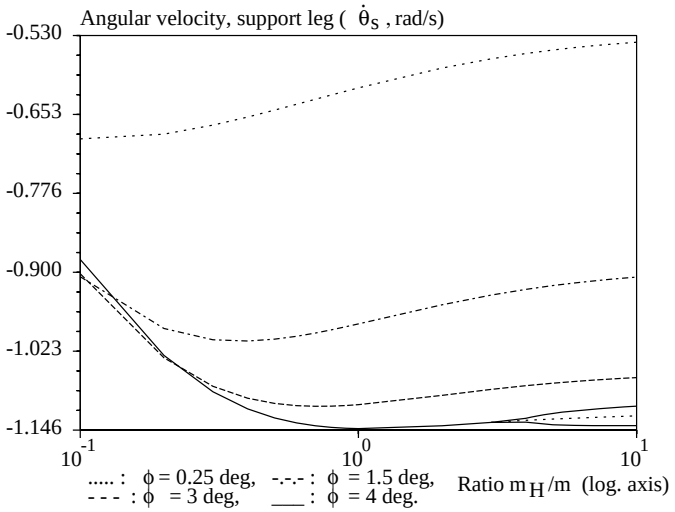

Figure C.14: *Bifurcation diagram* : angular velocity of the support leg $\dot{\theta}_s$ as a function of μ ($\beta = 1, \phi = 0.25^o, 1.5^o, 3^o$ and 4^o).

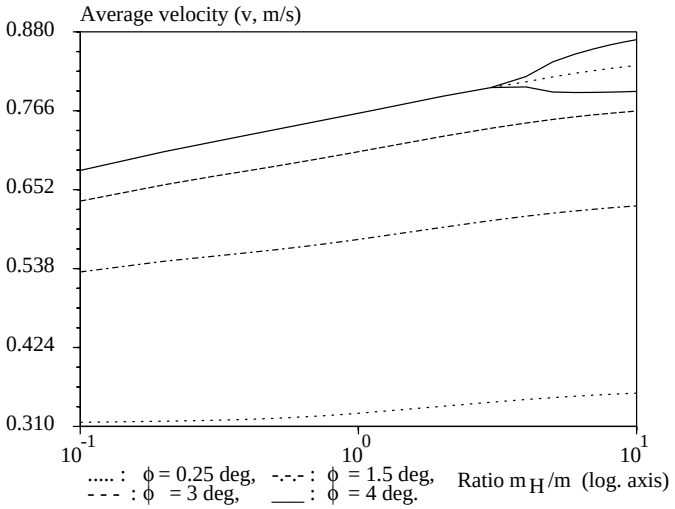

Figure C.15: *Bifurcation diagram* : average speed of progression v as a function of μ ($\beta = 1, \phi = 0.25^o, 1.5^o, 3^o$ and 4^o).

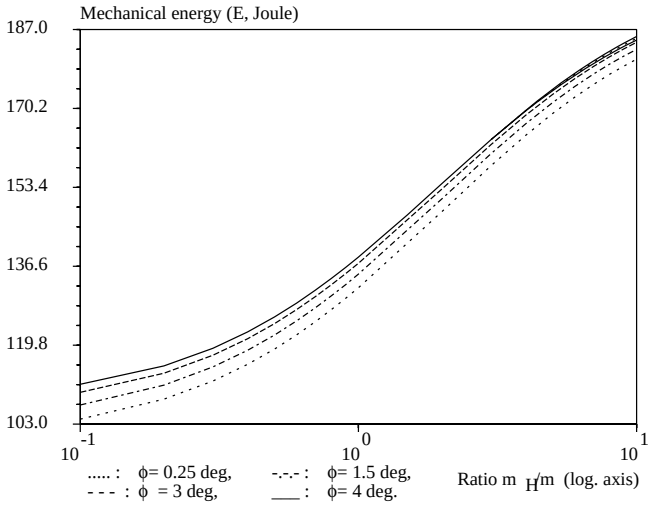

Figure C.16: *Bifurcation diagram* : mechanical energy E as a function of μ ($\beta = 1, \phi = 0.25^o, 1.5^o, 3^o$ and 4^o).

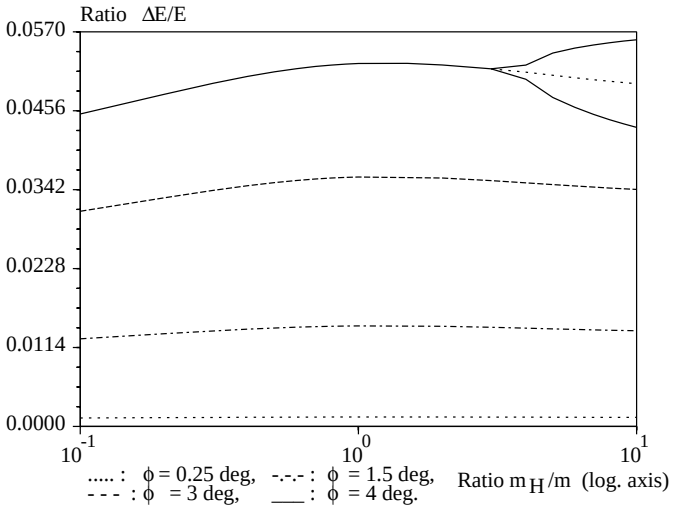

Figure C.17: *Bifurcation diagram* : ratio $\frac{\Delta E}{E}$ as a function of μ ($\beta = 1, \phi = 0.25^o, 1.5^o, 3^o$ and 4^o).

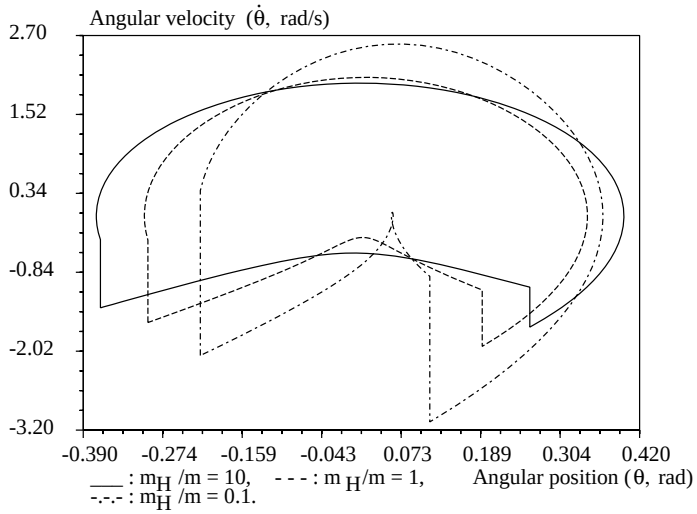

Figure C.18: *Phase plane limit cycles* for $\mu = 10$, $\mu = 1$ and $\mu = 0.1$ ($\beta = 1, \phi = 3^o$).

C.4 Bifurcation and phase plane diagrams related to the parameter β

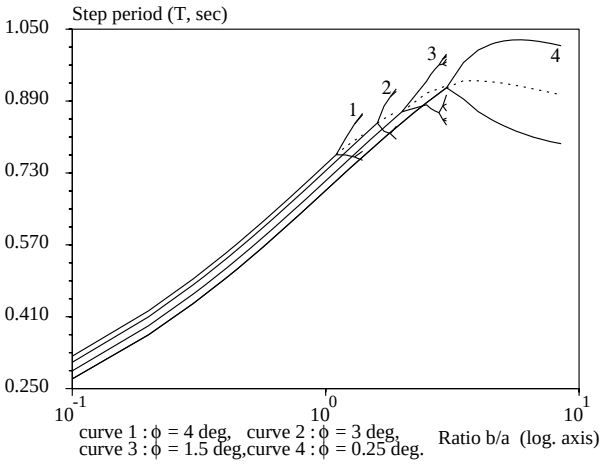

Figure C.19: *Bifurcation diagram* : step period T as a function of β ($\mu = 2, \phi = 0.25^o, 1.5^o, 3^o$ and 4^o).

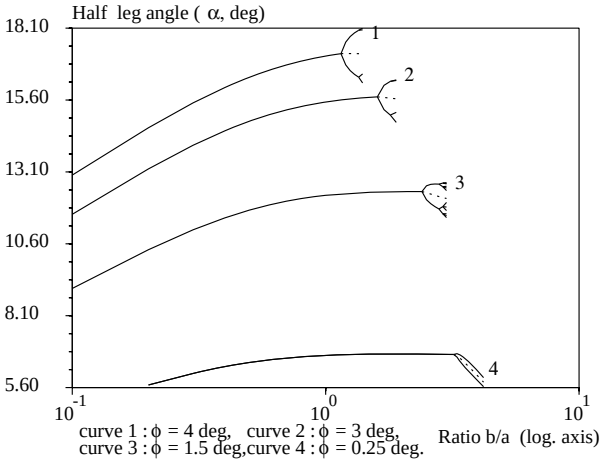

Figure C.20: *Bifurcation diagram* : half inter-leg angle α as a function of β ($\mu = 2, \phi = 0.25^o, 1.5^o, 3^o$ and 4^o).

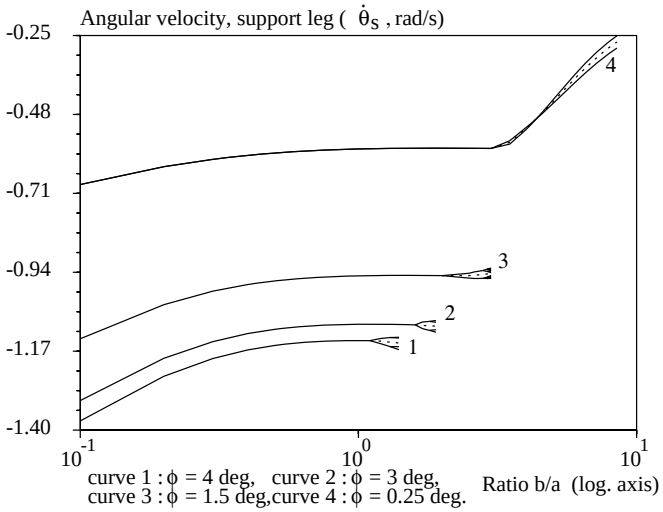

Figure C.21: *Bifurcation diagram* : angular velocity of the support leg $\dot{\theta}_s$ as a function of β ($\mu = 2, \phi = 0.25°, 1.5°, 3°$ and $4°$).

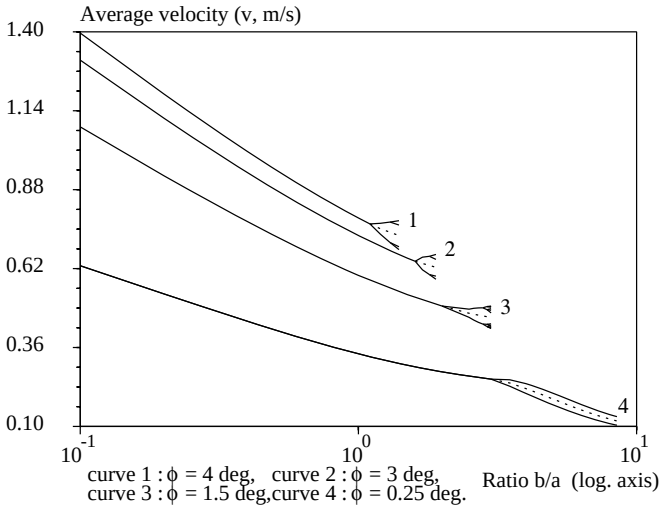

Figure C.22: *Bifurcation diagram* : average speed of progression v as a function of β ($\mu = 2, \phi = 0.25°, 1.5°, 3°$ and $4°$).

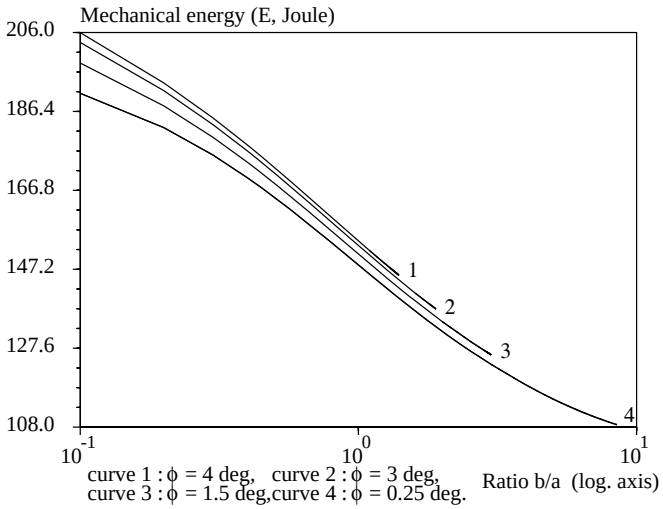

Figure C.23: *Bifurcation diagram* : mechanical energy E as a function of β ($\mu = 2, \phi = 0.25^o, 1.5^o, 3^o$ and 4^o).

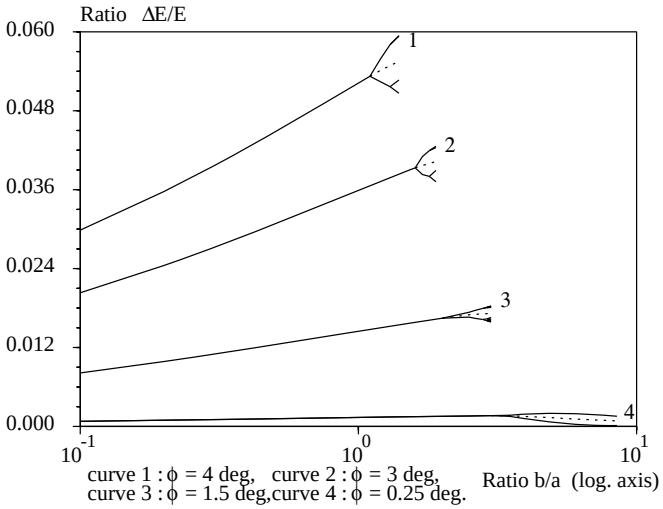

Figure C.24: *Bifurcation diagram* : ratio $\frac{\Delta E}{E}$ as a function of β ($\mu = 2, \phi = 0.25^o, 1.5^o, 3^o$ and 4^o).

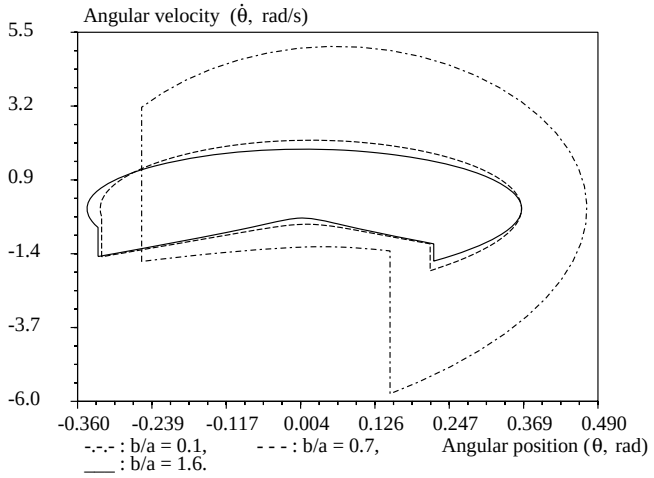

Figure C.25: *Phase plane limit cycles* for $\beta = 0.1$, $\beta = 0.7$ and $\beta = 1.6$ ($\mu = 2, \phi = 3^o$).

C.5 2^n-periodic and chaotic steady passive gaits

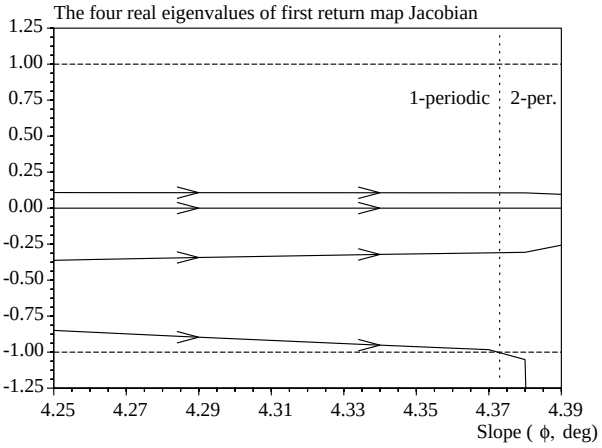

Figure C.26: *Transition from a 1-periodic to a 2-periodic steady gait:* behavior of the eigenvalues of the Jacobian matrix of the robot's Poincaré map.

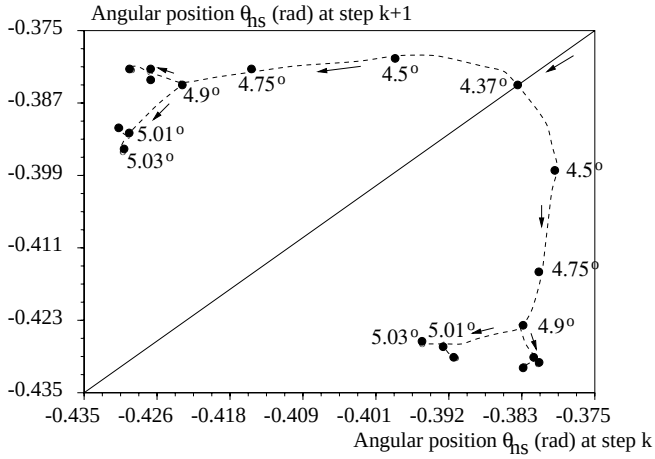

Figure C.27: 2^n*-periodic steady gait* $n \in \{0, 1, 2, 3\}$*, component* θ_{ns} *of the Poincaré map* ($\phi = 4.37^o$ to 5.03^o, $\mu = 2$, $\beta = 1$).

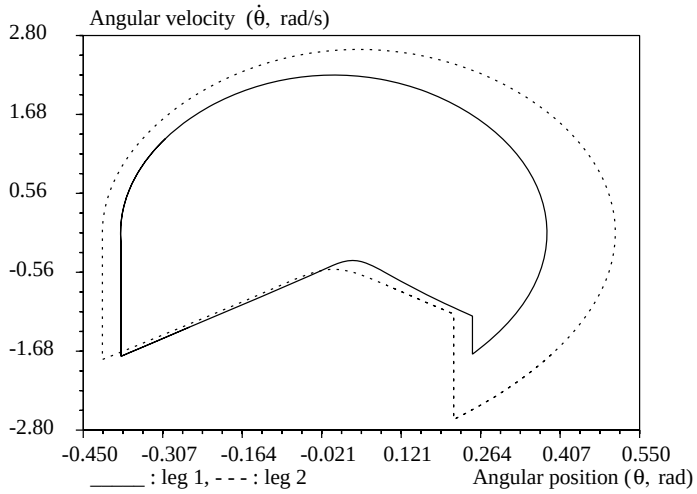

Figure C.28: *Phase plane limit cycles of a 2-periodic steady gait:* limit cycles associated with each leg, $\phi = 4.75^{\circ}$, $\mu = 2$, $\beta = 1$.

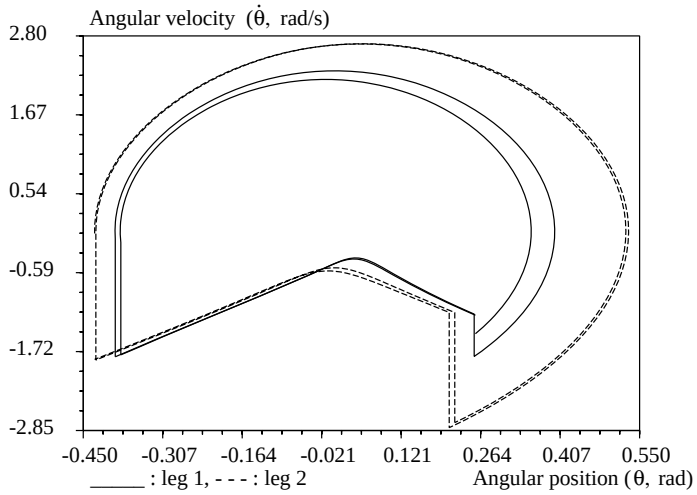

Figure C.29: *Phase plane limit cycles of a 4-periodic steady gait:* limit cycles associated with each leg, $\phi = 5^{\circ}$, $\mu = 2$, $\beta = 1$.

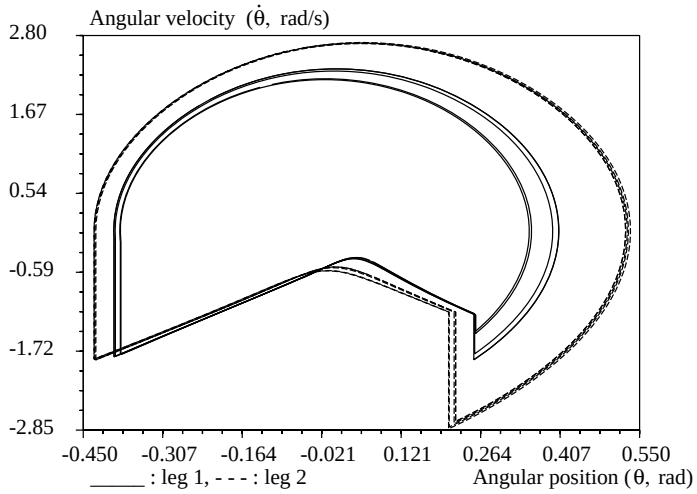

Figure C.30: *Phase plane limit cycles of a 8-periodic steady gait:* limit cycles associated with each leg, $\phi = 5.02^o$, $\mu = 2$, $\beta = 1$.

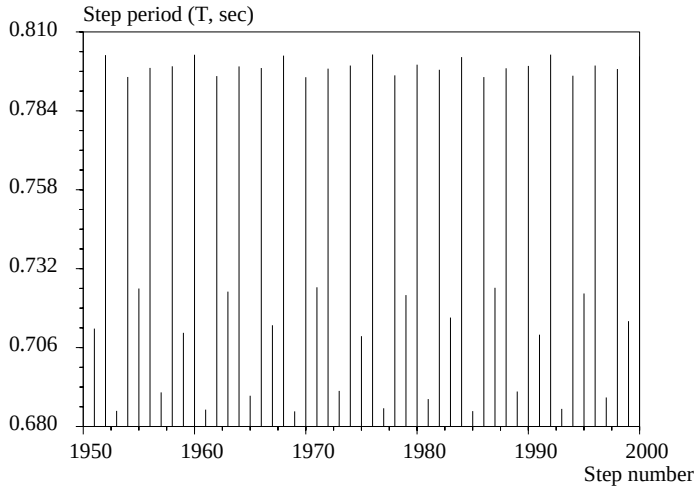

Figure C.31: 2^n*-periodic steady gait, n large:* periods of 50 consecutive steps ($\phi = 5.04^o$, $\mu = 2$, $\beta = 1$).

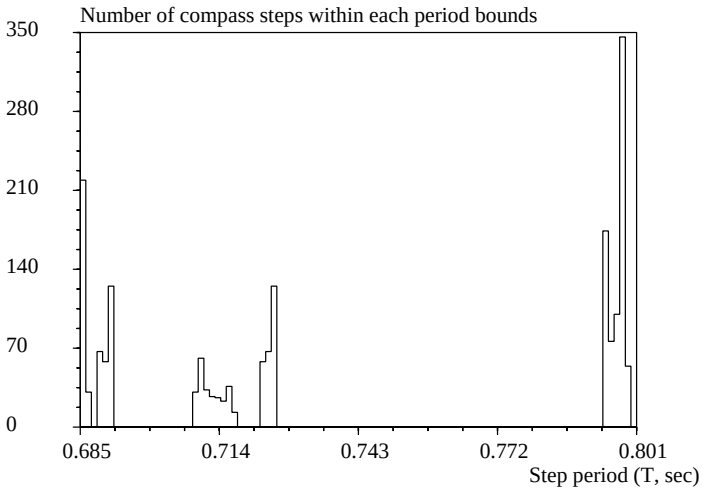

Figure C.32: 2^n*-periodic steady gait, n large:* histogram of the periods of 2000 consecutive steps ($\phi = 5.04°$, $\mu = 2$, $\beta = 1$).

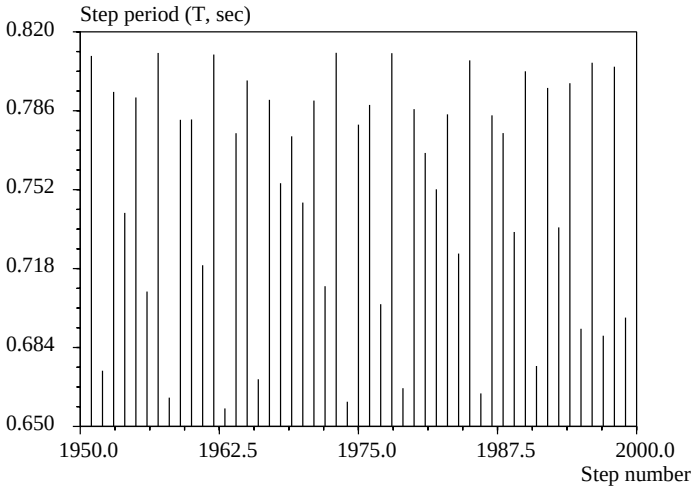

Figure C.33: *chaotic gait:* periods of 50 consecutive steps ($\phi = 5.2°$, $\mu = 2$, $\beta = 1$).

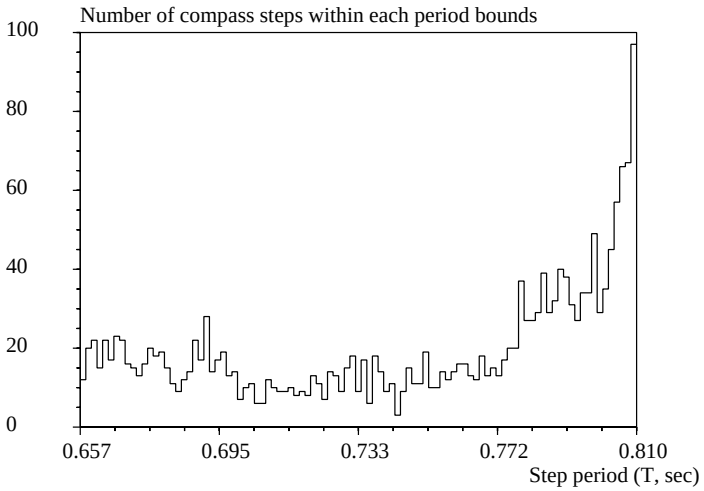

Figure C.34: *chaotic gait:* histogram of the periods of 2000 consecutive steps ($\phi = 5.2^o$, $\mu = 2$, $\beta = 1$).

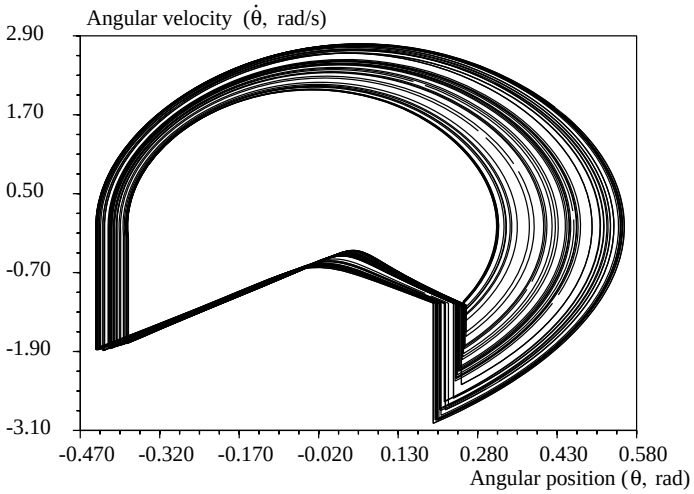

Figure C.35: *Phase plane trajectories of a chaotic gait associated with one leg,* 100 robot steps, $\phi = 5.2^o$, $\mu = 2$, $\beta = 1$.

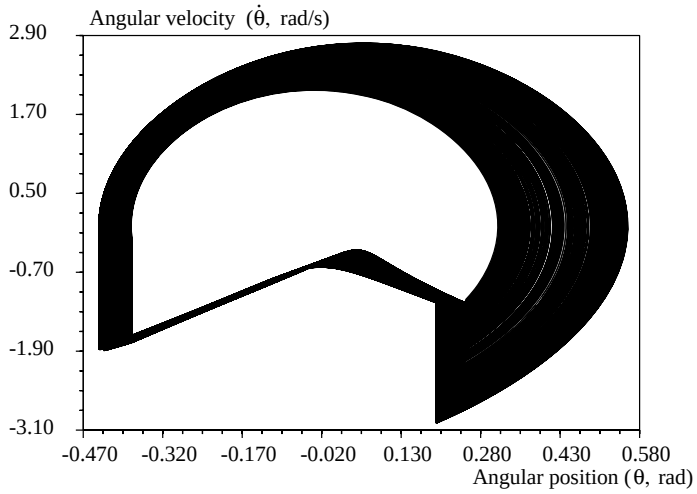

Figure C.36: *Phase plane trajectories of a chaotic gait associated with one leg,* 1250 robot steps, $\phi = 5.2^o$, $\mu = 2$, $\beta = 1$.

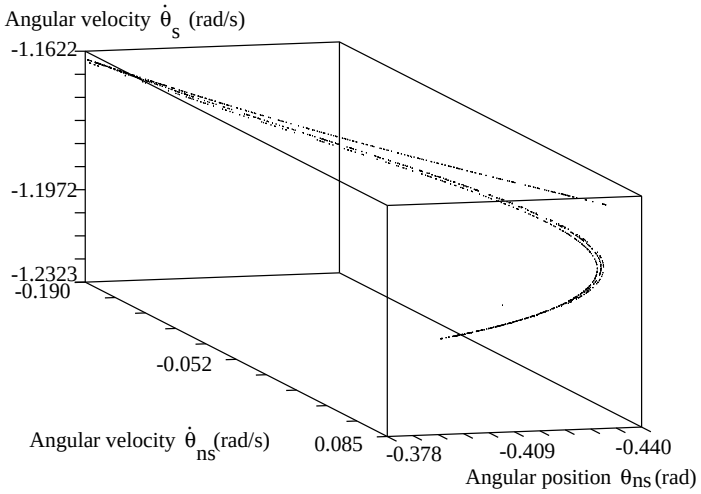

Figure C.37: *3D Poincaré section of a chaotic gait:* section along $\theta_{ns} + \theta_s = -2\phi$, i.e., at the beginning of a new step ($\phi = 5.2^o$, $\mu = 2$, $\beta = 1$).

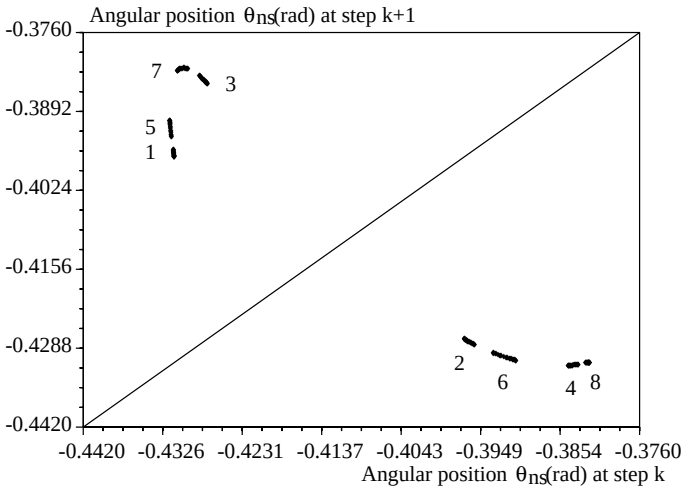

Figure C.38: *First return map of θ_{ns}:* 2^n-periodic steady gait, n large ($\phi = 5.04°$, $\mu = 2$, $\beta = 1$). The numbers indicate the sequence of visit of the 8 clusters.

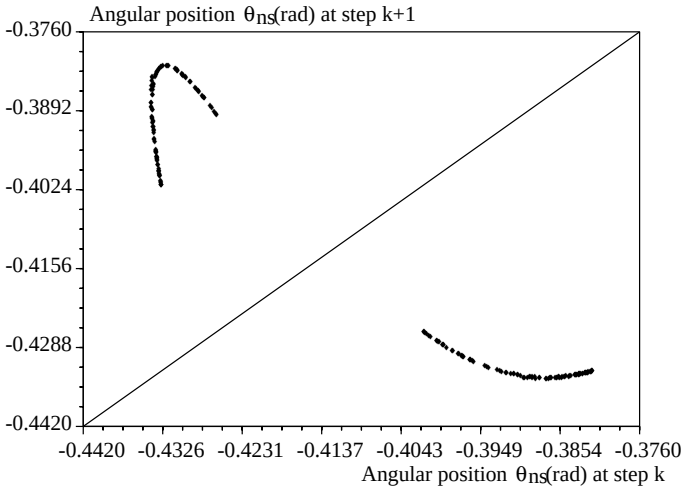

Figure C.39: *First return map of θ_{ns}:* 2^n-periodic steady gait, n very large ($\phi = 5.08°$, $\mu = 2$, $\beta = 1$).

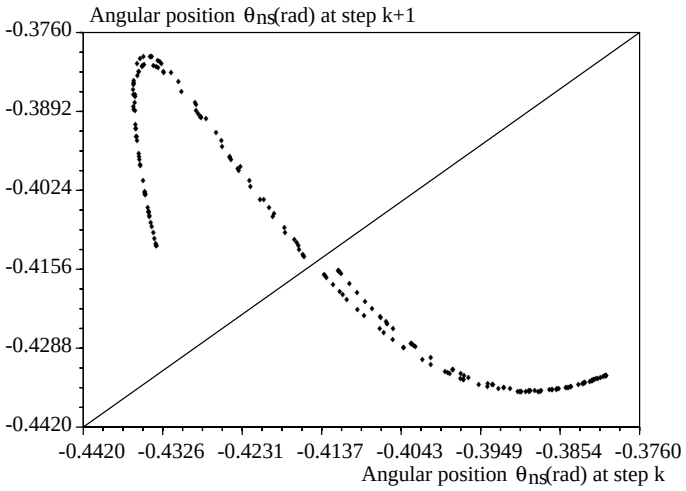

Figure C.40: *First return map of θ_{ns}:* approaching steady chaotic gait ($\phi = 5.12^o$, $\mu = 2$, $\beta = 1$).

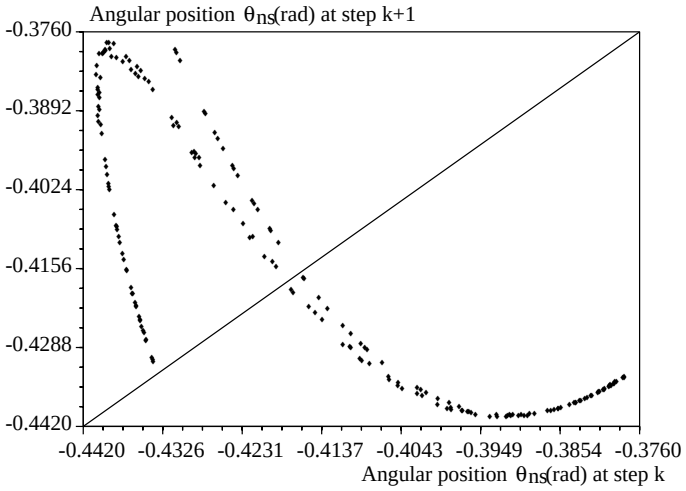

Figure C.41: *First return map of θ_{ns}:* steady chaotic gait ($\phi = 5.2^o$, $\mu = 2$, $\beta = 1$).

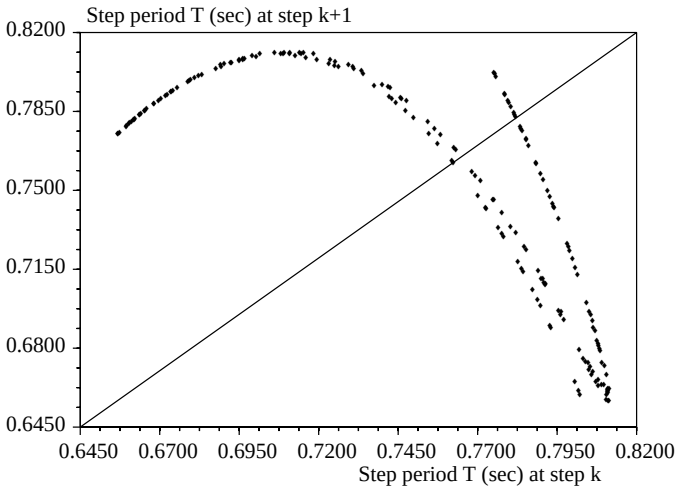

Figure C.42: *First return map of T:* steady chaotic gait ($\phi = 5.2^o$, $\mu = 2$, $\beta = 1$).

References

[BF92] M.D. Berkemeier and R.S. Fearing. Control of a two-link robot to achieve sliding and hopping gaits. In *Proc. of IEEE Conf. on Robotics and Automation*, volume 1, pages 286–291, Nice, 1992.

[BPV84] P. Bergé, Y. Pomeau, and C. Vidal. *Order within chaos.* John Wiley & sons, 1984.

[BS95] D.J. Block and M.W. Spong. Mechanical design & control of the pendubot. In *SAE Earthmoving Industry Conference*, Peoria, IL, 1995.

[BWH83] B. Bavarian, B.F. Wyman, and H. Hemami. Control of the constrained planar simple inverted pendulum. *Int. J. of Control*, 37(4):344–358, 1983.

[EG94] B. Espiau and A. Goswami. Compass gait revisited. In *Proc. IFAC Symposium on Robot Control (SYROCO)*, pages 839–846, Capri, Septembre 1994.

[Fra96] C. François. *Contribution à la locomotion articulée dynamiquement stable (in French).* PhD thesis, Ecole des Mines de Paris, April 1996.

[GCCR96] M. Garcia, A. Chatterjee, M. Coleman, and A. Ruina. Complex behavior of the simplest walking model. submitted to Journal of Biomechanics, 1996.

[GEK96] A. Goswami, B. Espiau, and A. Keramane. Limit cycle and their stability in a passive bipedal gait. In *Proc. of IEEE Conf. on Robotics and Automation*, pages 246–251, Minneapolis, april 1996.

[GFLZ94] A.A. Grishin, A.M. Formalsky, A.V. Lensky, and S.V. Zhitomirsky. Dynamic walking of a vehicule with two telescopic legs controlled by two drives. *The International Journal of Robotics Research*, 13(2):137–147, April 1994.

[GH77] C. L. Golliday and H. Hemami. An approach to analyzing biped locomotion dynamics and designing robot locomotion controls. *IEEE Trans. on Aut. Cont.*, 22(6):963–972, 1977.

[GH83] J. Guckenheimer and P. Holmes. *Nonlinear Oscillations, Dynamical Systems, and Bifurcations.* Springer-Verlag, New York, 1983.

[GKE96] A. Goswami, A. Keramane, and B. Espiau. Compass-like biped robot Part II: Control Strategies. Research report (to appear), INRIA, 1996.

[GR87] K. Gajewski and B. Radziszewski. On the stability of impact systems. *Bulletin of the Polish Academy of Sciences*, 35(3-4):183–189, 1987.

[Hay85] C. Hayashi. *Nonlinear Oscillations in Physical Systems*. Princeton Univ Press, NJ, 1985.

[HC92] Y. Hurmuzlu and T.H. Chang. Rigid body collisions of a special class of planar kinematic chains. *IEEE Transactions on Systems, Man and Cybernetics*, 22(5):964–971, 1992.

[Hec94] P.S. Heckbert (ed.). *Graphics Gems IV*. Academic Press Lim., 1994.

[Hil94] R. C. Hilborn. *Chaos & Nonlinear Dynamics*. Oxford University Press Inc., 1994.

[HM86] Y. Hurmuzlu and G.D. Moskowitz. The role of impact in the stability of bipedal locomotion. *Dynamics and Stability of Systems*, 1(3), 1986.

[KB91] D. Koditschek and M. Bühler. Analysis of a Simplified Hopping Robot *The International Journal of Robotics Research*, 10(6), 1991.

[KHRK81] J.A.S. Kelso, K.G. Holt, P. Rubin, and P.N. Kugler. Patterns of human interlimb coordination emerge from the properties of non-linear, limit cycle oscillatory processes: Theory and data. *Journal of Motor Behavior*, 13(4):226–261, 1981.

[Koo89] B. Koopman. *The three-dimensional analysis and prediction of human walking*. PhD thesis, University of Twente, The Netherlands, 1989.

[Map94] Maple V. *Waterloo Maple Software and the University of Waterloo,* 450 Phillip Street, Waterloo, Ontario, Canada, March 1994.

[MB91] R.T. McCloskey and J.W. Burdick. An analytical study of simple hopping robots with vertical and forward motion. In *Proc. IEEE Robotics & Automation*, volume 2, pages 1392–1397, Sacramento, April 1991.

[McG90] T. McGeer. Passive dynamic walking. *Int. J. of Rob. Res.*, 9(2):62–82, 1990.

[McM84] T.A. McMahon. *Muscles, Reflexes, and Locomotion.* Princeton University Press, 1984.

[OB93] J.P. Ostrowski and J.W. Burdick. Designing feedback algorithms for controlling the periodic motions of legged robots. In *Proc. IEEE Robotics & Automation*, volume 2, pages 260–266, Atlanta, May 1993.

[Ott93] E. Ott. *Chaos in Dynamical Systems.* Cambridge University Press, UK, 1993.

[PC89] T.S. Parker and L. O. Chua *Practical numerical algorithms for chaotic systems* Springer, Berlin, 1989.

[Rai86] M.H. Raibert. *Legged Robots that Balance.* MIT Press, Cambridge, USA, 1986.

[RG94] J. Rose and J.G. Gamble (eds). *Human Walking.* Williams & Wilkins, Baltimore, USA, 1994.

[Sci96] Scilab-2.2. *INRIA* Domaine de Voluceau, Rocquencourt, France, February 1996.

[Spo95] M.W. Spong. The swing up control problem for the acrobot. *IEEE Control Systems Magazine*, February 1995.

[TS91] H. Troger and A. Steindl. *Nonlinear stability and bifurcation theory.* Springer Verlag, Wien, 1991.

[VB90] A.F. Vakakis and J.W. Burdick. Chaotic motions in the dynamics of a hopping robot. In *Proc. IEEE Robotics & Automation*, volume 3, pages 1464–1469, Cincinnati, May 1990.

Unité de recherche INRIA Lorraine, Technopôle de Nancy-Brabois, Campus scientifique,
615 rue du Jardin Botanique, BP 101, 54600 VILLERS LÈS NANCY
Unité de recherche INRIA Rennes, Irisa, Campus universitaire de Beaulieu, 35042 RENNES Cedex
Unité de recherche INRIA Rhône-Alpes, 655, avenue de l'Europe, 38330 MONTBONNOT ST MARTIN
Unité de recherche INRIA Rocquencourt, Domaine de Voluceau, Rocquencourt, BP 105, 78153 LE CHESNAY Cedex
Unité de recherche INRIA Sophia-Antipolis, 2004 route des Lucioles, BP 93, 06902 SOPHIA-ANTIPOLIS Cedex

Éditeur
INRIA, Domaine de Voluceau, Rocquencourt, BP 105, 78153 LE CHESNAY Cedex (France)
ISSN 0249-6399